

This item was submitted to [Loughborough's Research Repository](#) by the author.  
Items in Figshare are protected by copyright, with all rights reserved, unless otherwise indicated.

## **A comparative study of the effect of varying wall heat flux on melting characteristics of phase change material RT44HC in rectangular test cells**

PLEASE CITE THE PUBLISHED VERSION

<https://doi.org/10.1016/j.ijheatmasstransfer.2019.07.038>

PUBLISHER

© Elsevier

VERSION

AM (Accepted Manuscript)

PUBLISHER STATEMENT

This paper was accepted for publication in the journal International Journal of Heat and Mass Transfer and the definitive published version is available at <https://doi.org/10.1016/j.ijheatmasstransfer.2019.07.038>.

LICENCE

CC BY-NC-ND 4.0

REPOSITORY RECORD

Fadl, Mohamed, and Philip C. Eames. 2019. "A Comparative Study of the Effect of Varying Wall Heat Flux on Melting Characteristics of Phase Change Material RT44HC in Rectangular Test Cells". figshare.  
<https://hdl.handle.net/2134/38301>.

# A comparative study of the effect of varying wall heat flux on melting characteristics of phase change material RT44HC in rectangular test cells

**Mohamed Fadl, Philip C. Eames**

Centre for Renewable Energy Systems Technology (CREST), Loughborough University, Loughborough (Leicestershire) LE11 3TU, United Kingdom

m.s.fadl@lboro.ac.uk; philip.c.eames@lboro.ac.uk

## **Abstract**

Results of an extensive experimental investigation performed to study the effect of different values of wall heat flux in a rectangular PCM (phase change material) test cell on the melting process are presented. A new experimental system consisting of a rectangular cross-section test cell formed from polycarbonate sheet, copper plates and mica heaters was constructed. During experiments uniform wall heat flux ( $q''_{\text{wall}}=675, 960 \text{ and } 1295 \text{ W/m}^2$ ) were applied to both the left and right sides of the test cell. Thermocouples were used to measure the temperature at different locations inside the PCM and on the surface of the copper plates and an infrared camera was used to measure the polycarbonate sheet external surface temperature distribution. The results show the expected strong correlation between the magnitude of wall heat flux and the melt fraction in the PCM as it drives the convective heat transfer. The transparent polycarbonate wall makes it possible to observe the location of the solid/liquid interface and determine melt fractions. The experiments have produced a significant experimental data set for the validation of numerical models simulating the solid/liquid phase change process and PCM melting in geometrical configurations relevant to, for example, latent heat thermal energy storage systems.

**Keywords:** PCM, Natural convection, Thermal energy storage, Heat Transfer.

## **Introduction**

Solar power technologies, both photovoltaic (PV) and solar thermal have improved in efficiency and performance over recent years, with a selection of systems available for commercial as well as residential applications. According to the International Energy Agency (IEA), renewable energy systems accounted for two-thirds of new power generation added to the world's electricity grids in 2016, with solar power being the fastest-growing source of new energy worldwide in that year, outstripping the growth in all other forms of power generation for the first time and leading experts to hail a “new era”[1].

In a solar thermal energy system, solar radiation is converted to heat using solar collectors. Since solar radiation varies with both time of the day and season of the year, employing a thermal energy storage system is essential if demand and availability are not concurrent, to allow for different weather conditions, enhance capacity factor and meet peak demands [2].

Latent heat thermal energy storage is one of the ways of storing thermal energy and can be used to help balance differences between heat/coolth generation and demand requirements with respect to disparities that occur in both time and magnitude. Thermal energy storage can allow collected and stored heat to be used at later times either on a diurnal or interseasonal basis. Generating and storing heat at periods of low demand and discharging at periods of high demand, allows the increased capacity factor to be achieved for a given collector system and reduces the need for required low utilisation plant to meet peak loads. Heat storage improves energy efficiency by utilising heat/coolth that would have been wasted. It

can also be used for the thermal management and cooling of electronic devices by reducing temperature rises during operation.

A PCM can effectively store or release latent heat during the melting or solidification process, respectively, and maintain the system temperature at/close to the melting/solidification temperature. Due to this, they have great potential for energy storage and environmental temperature control. Example applications include concentrated solar thermal power (CSP) systems, passive cooling, solar water/space heating and waste heat recovery [3].

The growth in interest in PCM applications has stimulated a need for better understanding of the heat transfer processes which take place during phase transitions. Research to date on PCM materials has concentrated on understanding the heat transfer characteristics of the PCM, specifically the effect of natural convection on the solid/liquid interface development and different techniques to improve the heat transfer between the PCM and the heat exchange surface and the heat transfer fluid (HTF).

In addition to the inherently transient nature, melting in PCMs is greatly affected by the dominant heat transfer mechanisms at a given time, conduction and/or convection. When analysing transient performance, isotherms, velocity vectors, solid/liquid interface location, melting rate, complete melt time and dimensionless parameters that describe the rate of heat transfer, i.e. the Nusselt number, can be used to characterise melting problems [4]. These quantities are however strongly influenced by the specific geometric configuration and thermal boundary conditions for each specific problem.

The geometric configuration and PCM enclosure orientation with respect to gravity affect the heat transfer mechanisms in the liquid zone which play a

significant role in the evolution of the shape, movement and morphology of the solid/liquid interface, which in turn affects the heat transfer and the melting process within the PCM. An overview of melting in different types of enclosures is given in the reviews by [5], [6], [7],[8], and [9].

For enclosures with vertical walls that are heated, the melting rate is higher in the upper portion of the containers due to natural convection in the melt. Increasing the height/width ratio of the enclosures for the same volume in general augments the buoyancy effect and results in a faster melt process and a decrease in charging time [4].

Melting of phase change materials in rectangular cross-section containers has attracted significant interest due to its wide-ranging engineering applications in such fields as casting, metallurgy, spacecraft and avionics thermal control, military electronic systems, power electronic equipment, personal computing and communication equipment and thermal energy storage.

There are three main ways to predict and better understand the heat transfer processes which take place during phase transitions, i.e. Analytical, Experimental and Numerical (via simulation). Analytical solution of the melting problem is problematic due to the complex nature of the heat transfer and the moving phase transition. In 1891 Stefan presented a mathematical solution to the phase change problem of ice formation in simple geometries [10]. Due to the lack of an unstable analytical solution for the analysis of heat transfer in complex thermal energy storage systems, various researchers have investigated the system performance numerically [11].

Pal and Joshi [12] studied computationally and experimentally the melting of an organic (PCM) (n-triacontane) in a side-heated tall enclosure with an aspect ratio

of 10. They reported that natural convection plays a dominant role during the initial stages of melting and that the strength of natural convection diminishes as melting is completed.

Bashar and Siddiqui [13] conducted an experimental study to investigate the transient melting and heat transfer of a nanoparticle-PCM mixture in a rectangular enclosure using four types of nanoparticles (silver, copper oxide, aluminium oxide and multi-walled carbon nanotubes) with paraffin wax used as the PCM. The results show that all four nanoparticle-enriched PCM mixtures provided better thermal performance when compared to the case with the plain PCM due to increased thermal conductivity.

Kamkari and Shokouhmand [14] carried out an experimental investigation of phase change material (PCM) melting in a transparent rectangular test cell with and without horizontal fins. The test cell was heated isothermally from one side while the other walls were insulated to reduce thermal losses. Experiments were performed with wall temperatures set at 55, 60 and 70 °C. The experimental results indicated that increasing the number of fins decreased the required time for melting and increased the total heat transfer rate while the surface-averaged Nusselt number reduced.

Dhaidan et al [15] experimentally and numerically studied melting of n-octadecane with CuO nanoparticle suspensions in a square cross-section enclosure subjected to a constant heat flux on one side wall. The experimental and numerical results indicate that the nanoparticle loading has a positive effect on raising the thermal conductivity of the PCM/nanoparticle composite, increasing the heat transfer within the composite resulting in a decreased the charging time.

Kamkari et al [16] experimentally investigated the transient thermal behaviour of PCM melting in a rectangular test cell at different inclination angles. The enclosure was heated isothermally from one side while the other walls were insulated to reduce heat losses. The experiments revealed that the enclosure inclination had a significant effect on the development of natural convective heat transfer and consequently on the heat transfer rate and required melting time for the PCM.

Yanxia et al [17] conducted an experimental investigation to examine the thermal characteristics of the melting process in a rectangular enclosure heated from a single vertical side. They used a novel PCM ethanolamine–water binary mixture which has a high-Prandtl number, their experiments indicated that the natural convection in the liquid enhanced the melting process compared to pure conduction.

Hamad et al [18] experimentally investigated the melting process of polyethylene glycol 1500 (PEG 15500) in a rectangular enclosure. Their experiments show a strong correlation between the hot wall temperature and the developments of the melt fraction, expected a hot water temperature strongly influences the convective heat transfer. The cold wall temperature had an insignificant effect on the development of the PCM melt with time for a constant hot wall temperature. The melting rate had the same characteristic form for all cold wall temperatures used in their study.

Motahar et al [19] presented an experimental investigation into the melting process of the PCM n-octadecane with titanium oxide ( $\text{TiO}_2$ ) nanoparticles dispersed through it in a rectangular enclosure heated at a constant rate from one vertical side. Their experiments showed that during the initial stage of melting, heat is transferred by conduction while at later times natural convection dominates

the heat transfer. Dispersing  $\text{TiO}_2$  nanoparticles through the PCM led to an increase in the Bingham number and consequently the natural convection and melting rate reduced.

Melting of phase change materials in a vertical tube or vertical cylinder (having a circular cross-section) is affected by the orientation of the symmetry axis of the cylindrical vessel to the gravity vector [4].

Jones et al [20] conducted an experimental study of the melting of n-eicosane in a vertical cylindrical enclosure, and a numerical investigation of the melting process when the enclosure was heated isothermally from the sides, with a constant temperature maintained at the bottom and insulated at the top. It was shown from the experiments that four distinct regimes occurred during the melting process which were: (a) pure conduction, (b) mixed convection/conduction, (c) convection dominant, and (d) “shrinking solid”.

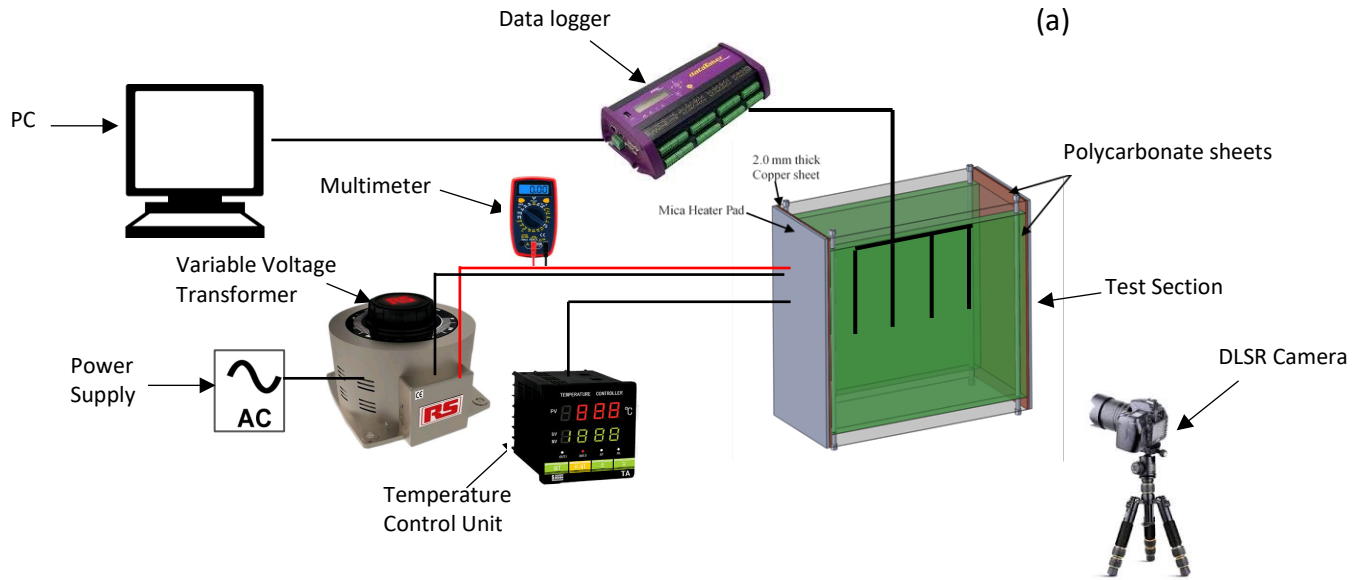
In the current research, the melting process of phase change material RT44HC has been evaluated experimentally for a test cell of rectangular cross-section subject to a uniform wall heat flux applied to both the left and right vertical sides, while the other wall conditions are essentially adiabatic. Both qualitative and quantitative approaches have been employed by visually observing the movement of the solid-liquid interface with time and measuring the temperature distribution within the PCM with an array of thermocouples.

## **Experimental apparatus**

A rectangular test cell filled with phase change material that can be subjected to uniform wall heat flux from both left and right vertical sides has been fabricated from transparent polycarbonate to allow the accurate measurement of the effect of



input wall heat flux intensity on the transient solid-liquid interface movement and temperature distribution within the PCM.



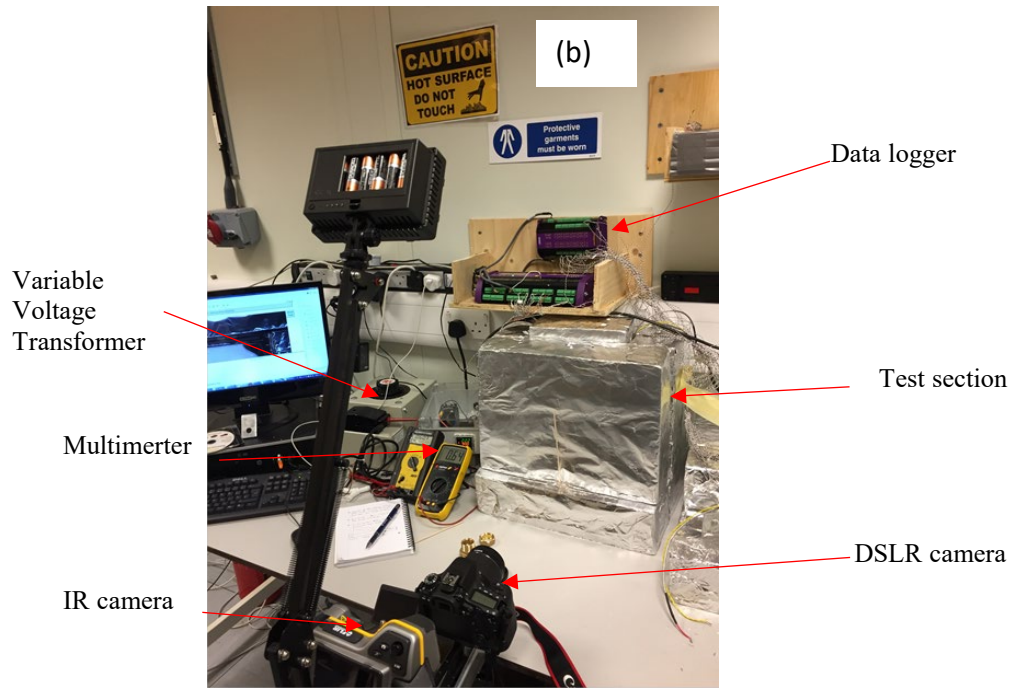


Figure1. (a) Schematic diagram of the experimental test rig, (b) picture of the laboratory setup.

The developed experimental test rig is shown in Fig.1 and comprises the rectangular PCM test cell, insulation, power supply, voltage transformer, thermocouples, temperature control unit, data acquisition system, DSLR camera, Infrared camera and a computer.

The rectangular test cell was formed from 12 mm thick transparent polycarbonate sheet [21] to allow observation of the melt fraction development in the RT44HC during the experiment. The internal dimensions of the test cell were 176 mm high, 200 mm wide. The depth of the test cell was 100 mm, this depth was considered to be sufficiently large that the boundary effects at the midplane induced by the front and back walls as shown in Fig.2 would be negligible. The thermal conductivity of polycarbonate is approximately 0.19 W/m K with a maximum operating temperature of 150 °C and a density of 119 kg/m<sup>3</sup>. Four holes

in the upper side of the test cell were used to introduce the liquid PCM into the store and to provide space for thermal expansion of the PCM that occurs during the melting process. Thin 2 mm thick copper plates [22] with an area of 100 x 200 mm from the right and left vertical sides of the test cell on which Mica heating pads are mounted to provide uniform wall heat flux to the plates. Copper plates were used for the end walls due to compatibility with the PCM, its long life and high thermal conductivity 401 W/m K. The Mica heater which could operate up to a maximum voltage of 240 VAC was connected to an adjustable AC power supply to allow heat input rate to be varied.

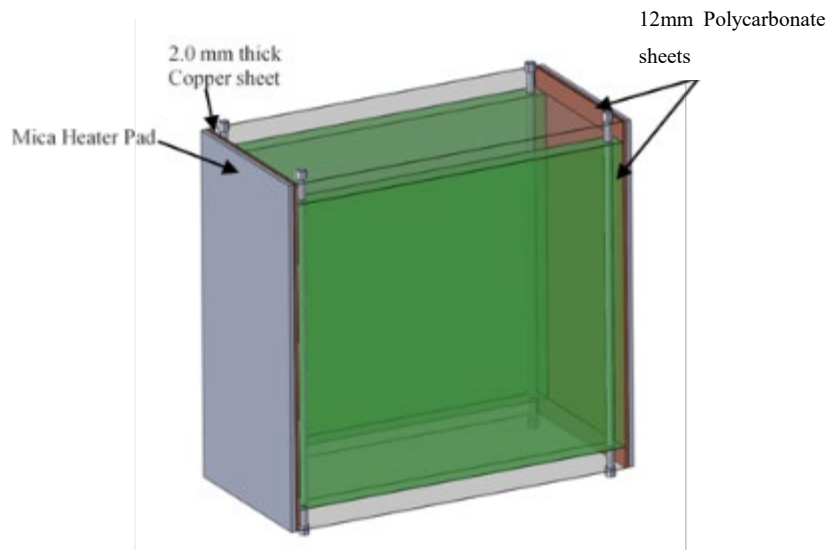


Figure 2. Schematic diagram of the rectangular cross-section test cell.

The Mica heaters were attached to the copper plates using epoxy adhesive with high thermal conductivity silicone thermal grease used to eliminate air pockets and ensure good contact, and thermal contact. 12 T-type thermocouples formed from 0.26 mm diameter wire with a calibrated accuracy of  $\pm 0.3$  °C were placed in 4 columns and 3 rows in the vertical middle plane of the test cell as shown in Fig.3 These were connected to a data logger and temperatures were recorded during the melting process. Fig.4 shows the location of the three thermocouples secured to

each copper plate with the conductive epoxy resin used to measure surface temperature. Two additional thermocouples located outside the test cell were used to measure the ambient and insulation temperatures.

A sheet of Kingspan Kooltherm [23] of thickness 100 mm and thermal conductivity of 0.018 W/m K was used to provide thermal insulation on all sides of the test cell. A data acquisition (DAQ) unit, DT85 providing 48 common referenced analogue input channels [24] was used to log the temperature readings. The DAQ unit was connected to a personal computer via a USB port and the dEX software platform was used to configure and manage the logger in real time. The temperatures were recorded at intervals of 10 seconds for the full duration of the experiment.

In order to record the development and movement of the solid/liquid interface during melting, a Canon 24.2 Megapixel digital camera, Canon EOS 80D [25] with a 18-55 mm lens was used to take photographs every 30 minutes. The camera mounted on a tripod was fixed places at a distance of 50 cm from the PCM test cell. A light source behind the test cell was used to make the solid/liquid interface more visible. An infrared camera, FLIR B series [26] with a resolution of 320 by 240 Pixels was mounted in the front of the test cell to record the temperature field.

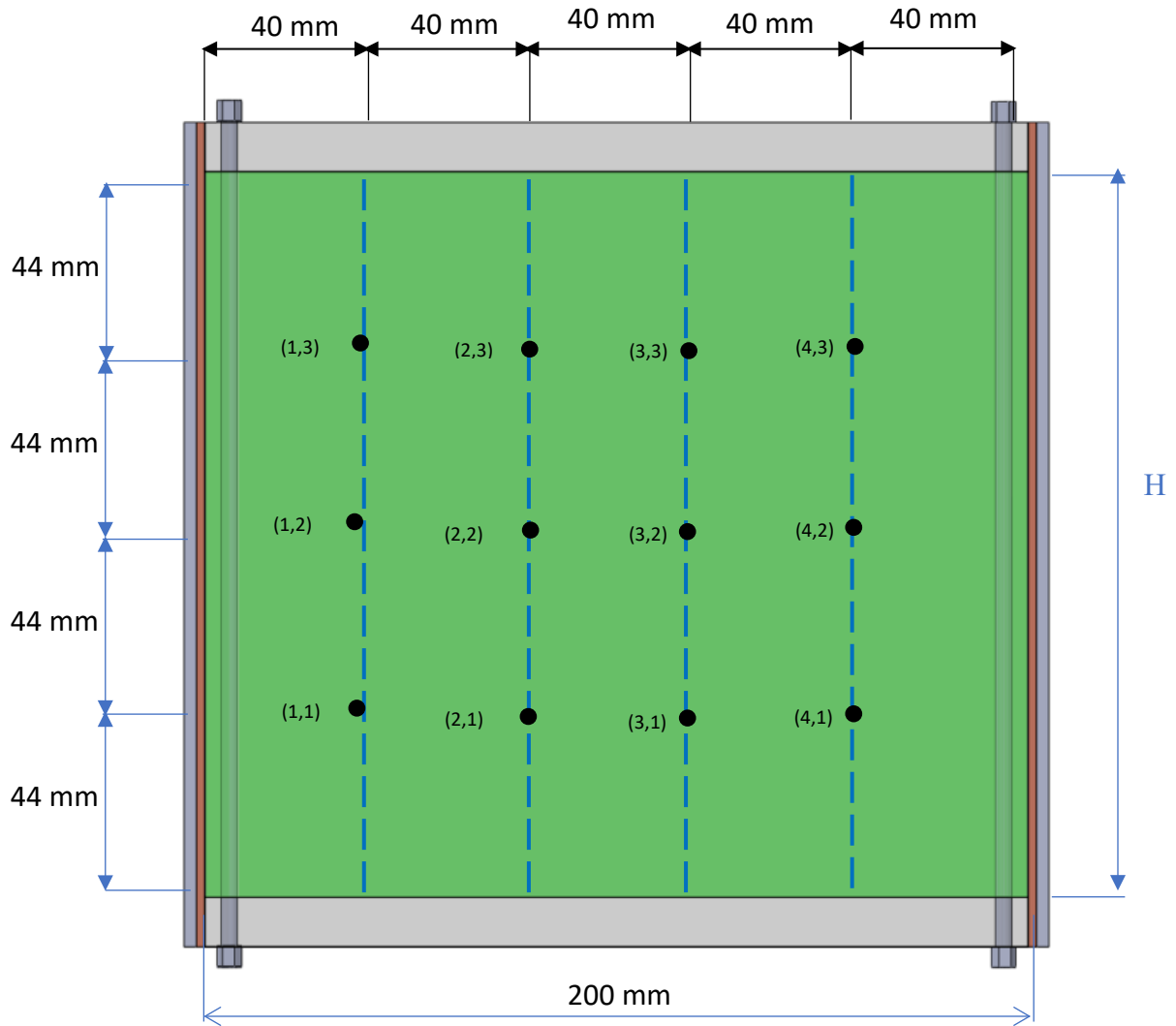


Figure 3. Thermocouples locations in the mid-plane of the PCM container.

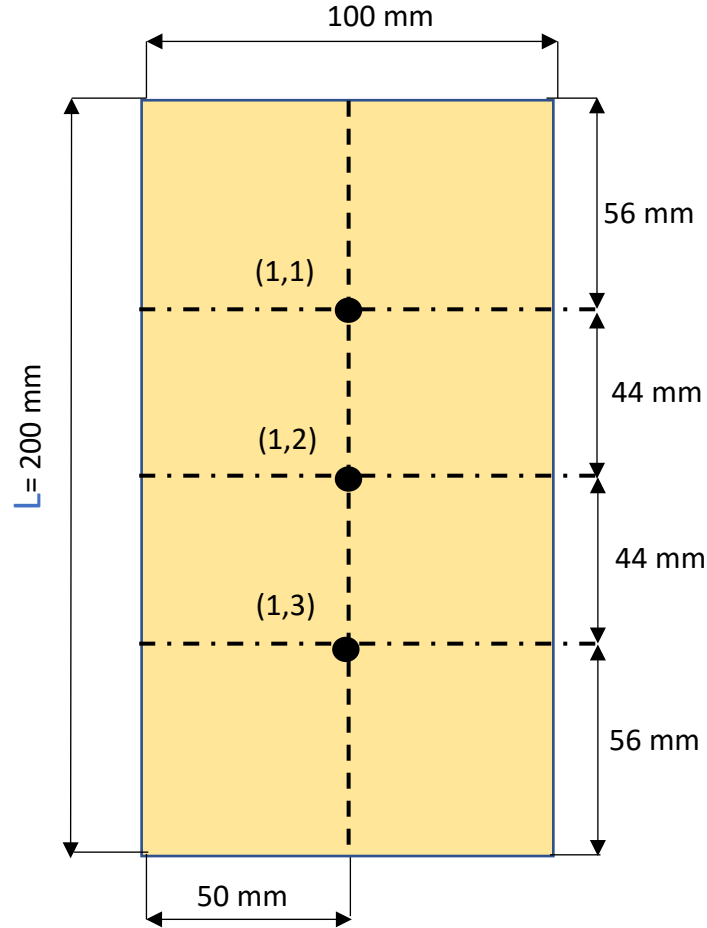


Figure 4. The locations of the three thermocouples used to measure the surface temperature of the heating plates.

### Experimental test procedure

The PCM was initially melted in an oven and poured into the test cell in thin layers, with each layer allowed to solidify prior to the next being introduced. This process was continued until the test cell was filled totally with PCM. The objective of this filling procedure was to ensure that no air pockets formed inside the solid PCM. After filling, the test cell was kept at room temperature (20°C to 22°C) for at least 24 hrs to ensure that all of the solid PCM was at the same temperature. At this time, the temperature difference between all thermocouple measurements in the PCM was less than 0.1 °C.

## Data Reduction

### Absorbed energy

To determine the amount of energy absorbed by the PCM, both sensible and latent heats were calculated at every data acquisition period. Total sensible heat gain **for the liquid and solid regions were** calculated by using equation (1) [27]:

$$Q_{sensible,PCM}(t) = \int_{V_{liq}(t)} \rho_s C_s (T_{m1} - T_i) dV_{liq} + \int_{V_{liq}(t)} \rho_{liq} C_{liq} (T_{mean_{liq}}(t) - T_{m2}) dV_{liq} + \int_{V_s(t)} \rho_s C_s (T_{mean_s} - T_i) dV_s \quad (1)$$

Where  $T_{mean_{liq}}(t)$  and  $T_{mean_s}(t)$  represent the instantaneous mean temperatures of liquid and solid phases, which were calculated by averaging the temperatures of thermocouples located in each phase using equations (2) and (3):

$$T_{mean_{liq}}(t) = \frac{1}{n_l(t)} \sum_{i=1}^{n_{liq}(t)} T_i \quad (2)$$

$$T_{mean_s}(t) = \frac{1}{n_s(t)} \sum_{i=1}^{n_s(t)} T_i \quad (3)$$

Where  $n_{liq}(t)$  and  $n_s(t)$  represent the number of thermocouples located in each of the liquid and solid regions of the PCM at each measurement time, respectively.

The latent heat of the region related to the thermocouple was calculated using equation (4):

$$Q_{Latent,PCM}(t) = f M_{PCM} h_{latent} \quad (4)$$

where  $f$  is the value of the liquid fraction percentage

The total energy absorbed by the PCM for the liquid and solid regions can then be calculated by the sum of the latent and sensible heats which have been estimated by equations (1) and (4).

$$Q_{total,PCM}(t) = Q_{sensible,PCM}(t) + Q_{latent,PCM}(t) \quad (5)$$

A simple heat balance, equation (6) can be used to evaluate the surface-averaged natural convective heat transfer coefficient during melting.

$$\bar{h}(t) = \frac{Q_{total,PCM}(t)}{A_w(T_w - T_m)\Delta t} \quad (6)$$

Where  $Q_{total,PCM}(t)$  is the total heat transfer from the hot walls to the PCM during the time interval ( $\Delta t$ ).  $A_w$  is the total surface area over which the heat flux is provided.  $T_w$  is the average heated wall temperature and  $T_m$  is the solid-liquid interface temperature which was considered to be the melting temperature of the PCM.

The dimensionless average Nusselt number, based on the characteristic length of the test cell (height  $H$ ) can be written as equation (7):

$$\overline{Nu}_{(t)} = \frac{\bar{h}_{(t)}H}{K_{liq}} \quad (7)$$

The relevant dimensionless numbers are the Stefan number  $Ste$ , Rayleigh number and the Fourier number  $Fo$  [11]:

$$Ste = \frac{c_{p,l} q'' H}{K h_{latent}}, \quad Ra = \frac{\rho_l^2 c_{p,l} g \beta H^4 q''}{\mu k^2}, \quad Fo = \frac{K t}{\rho c_{p,l} H^2} \quad (8)$$



## Input power

The experiments were conducted at three different input power rates 27, 38.4 and 51.8 Watts (corresponding to a heat flux of 675, 960 and 1295 W/m<sup>2</sup>), the constant wall heat flux,  $q''$  to the test cell was calculated based on the electric power dissipated over the heat transfer surface area and is given in the equation (9):

$$q'' = \frac{IV}{A_w} = \frac{IV}{2 LW} \quad (9)$$

where  $A_w$  is the total surface area of both heaters providing the heat flux to the system.

The key dimensionless numbers for each of the experiments are listed in Table 1.

Table 1 Key dimensionless numbers for the three experiments.

Experiment Number	$q''$	Ra ( $\times 10^{10}$ )	Ste
1	675	5.04	5.44
2	960	7.17	7.74
3	1295	9.67	10.45

## Phase change material used

RT44HC a commercially available material (Rubitherm GmbH-Germany) [28] was used for these experiments because it has a high latent heat of fusion, is chemically stable, does not degrade over multiple cycles, is non-corrosive, and non-toxic. This material has a high heat storage capacity over a narrow temperature range which makes it suitable for solar energy, domestic hot water and space heating applications.

In order to determine the specific heat capacity of the PCM during the melting process, measurements were performed using a TA Instruments Differential

Scanning Calorimeter (DSC)[29] with an average error of less than 1.0% and a liquid nitrogen cooling system. The measurements were performed with heating/cooling rates of 1 °C.min<sup>-1</sup>, 5 °C.min<sup>-1</sup> and 10 °C.min<sup>-1</sup> and a temperature range from 20-70 °C. The measured temperature enthalpy curve recorded during the melting process for RT44HC is shown in Fig.5. The measured temperature range for RT44HC over which melting occurred was 42.13 to 43.28 °C. The measured latent heat was 218110 J/kg for a heating rate of 1 °C.min<sup>-1</sup>. The other thermo-physical properties of RT44HC were obtained from the manufacturer's data sheet [28] and are presented in Table 2.

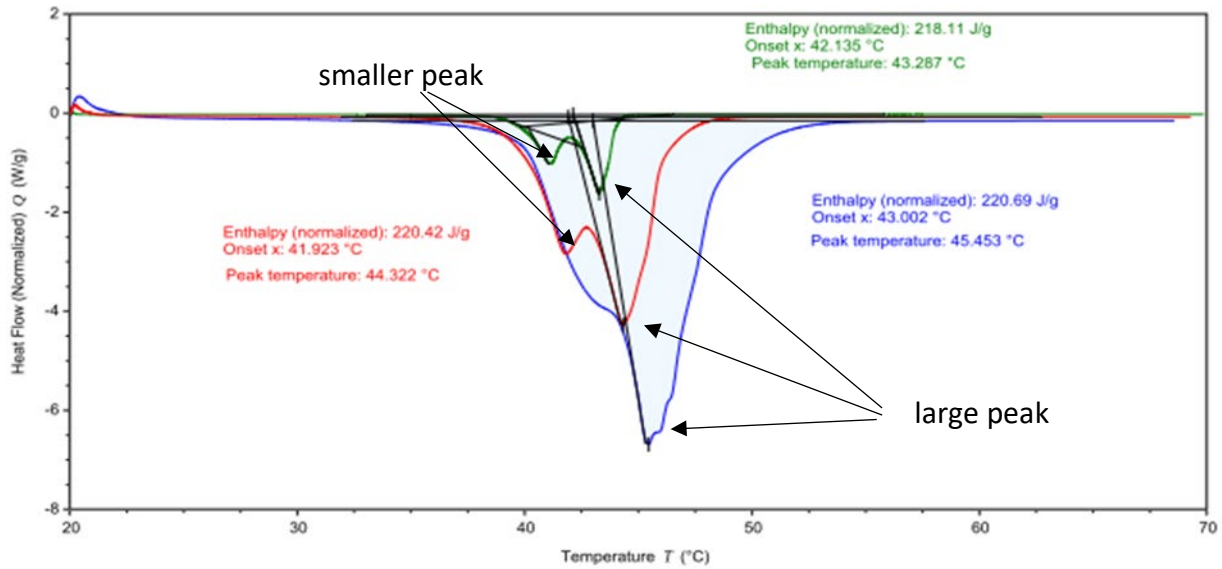


Table 2 Thermophysical properties of paraffin wax RT44HC [25].

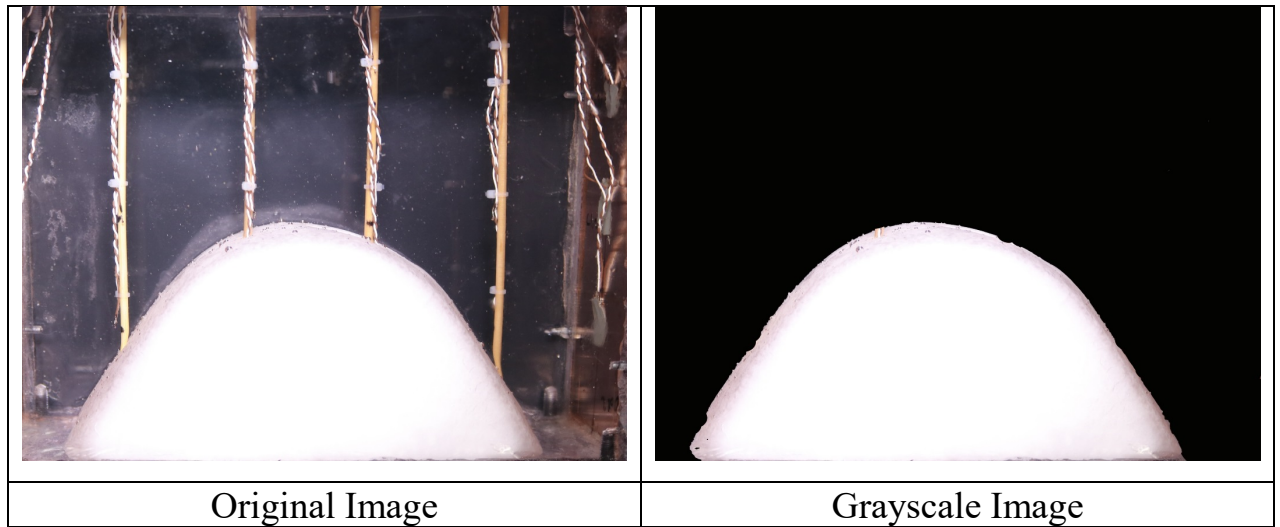
Thermal conductivity ( $k_s$ )	0.2 W/m K
Thermal conductivity ( $k_{liq}$ )	0.2 W/m K
Specific heat of solid phase ( $C_p$ ) <sub>s</sub>	2000 J/kg K
Specific heat of liquid phase ( $C_p$ ) <sub>liq</sub>	2000 J/kg K
Density: solid phase ( $\rho_s$ )	800 kg/m <sup>3</sup>
Density: liquid phase ( $\rho_{liq}$ ),	$\rho(T) = -0.6698 T + 992.61$ kg/m <sup>3</sup> , $T(k)$
Volumetric expansion coefficient ( $\beta$ )	0.00137 K <sup>-1</sup>
Dynamic viscosity ( $\mu_{liq}$ )	0.008 kg/m s

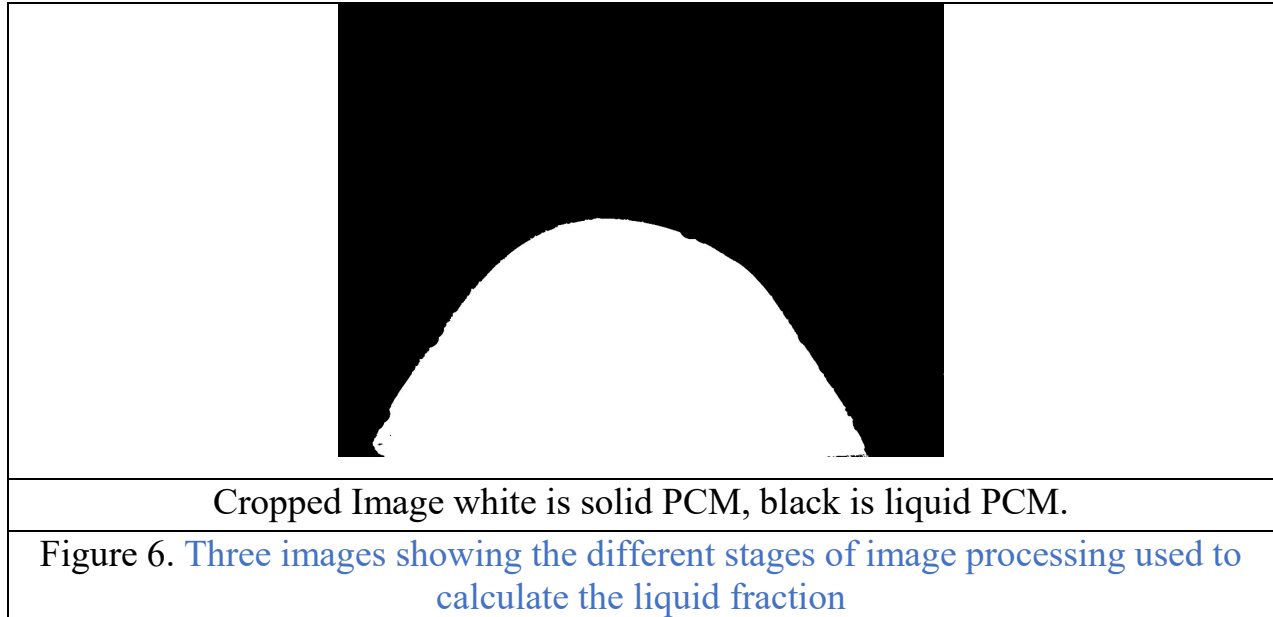
## Melt front evolution

To evaluate the melt fraction and the location of the moving solid-liquid interface, the insulation on the front face of the test cell was periodically removed every 30 minutes and a colour digital image taken. The image was converted to a black and white image which contains a two-dimensional array of either zeros or ones corresponding to black and white pixels respectively. The MATLAB image processing toolbox [30] was utilized to determine the instantaneous liquid fraction based on the number of zeros and ones in the array. The liquid fraction was evaluated by dividing the number of zeros in the array by the total number of pixels forming the image.

$$f = \frac{NP_0}{NP_t} \quad (10)$$

where  $NP_0$  and  $NP_t$  are the number of 0 values in the array and the total number of points in the array, respectively. Fig.6 shows the steps used for calculated the liquid fraction.





### Calibration of infrared images

In the experiments, the temperatures measured by the thermocouple probes can only reflect the temperatures at spot locations, using thermocouples it is very difficult to unobtrusively obtain the temperature field of the entire domain. Additional information about the temperature field was obtained by using an infrared camera focused on the outside front face of the PCM test cell. The test cell surface must be exposed to the infrared camera for temperature measurement, with a consequent heat loss from the higher temperature test cell surface to the ambient, resulting in a lower temperature being measured than if insulation remained in position. To minimize this, the insulation was removed and replaced rapidly. To ensure consistency between thermocouple measurements and the images taken with the infrared camera, a calibration between the two sets of temperature measurements was performed. At 30 min intervals, an image was taken of the PCM test cell surface with the infrared camera and compared to measurements simultaneously made with the thermocouples. The temperatures measured with the IR camera and the thermocouple measurements are presented as plots of

temperature against time in Fig.7 (a–d). In all cases, good agreement is seen between the thermocouples and infrared measurements up to about 40 °C i.e. while the PCM is solid. Above this temperature, a systematic deviation is seen between the two sets of temperature measurements suggesting that the liquid state of the PCM is affecting the temperature measured by the infrared camera, it is possible to compensate for the difference between infrared readings and the thermocouples reading to given consistent temperature data sets with an accuracy of  $\pm 1.0$  °C.

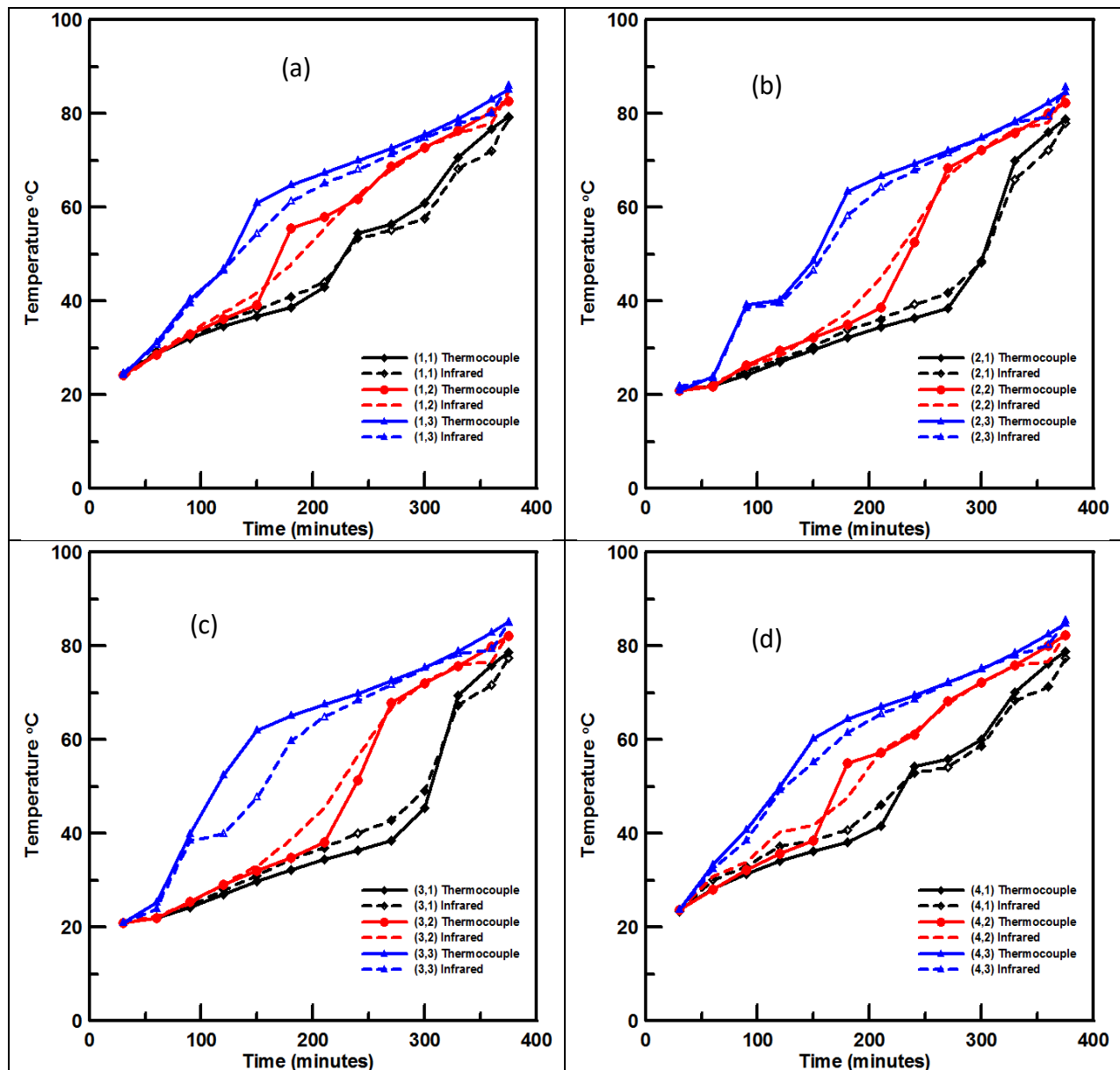


Figure 7. The infrared and thermocouple determined temperatures recorded for a wall heat flux  $q''=1295 \text{ W/m}^2$ .

## Results and discussion

To confirm the performance of the developed experimental setup with heating from two sides, initial experiments were performed to check that melting occurred symmetrically. Fig.8 presented the measured temperatures with time from the thermocouples on the heated walls with a heat flux input of  $960 \text{ W/m}^2$  applied to the left and right sides of the test cell. For all locations at each side, similar temperatures were recorded confirming symmetrical behaviour. In the early stage of heating and the initial PCM melting phase ( $< 60$  minutes) the heat transfer is conduction dominated in the PCM and the heated surface temperatures in the vertical direction are similar. After 60 minutes, the liquid PCM layer adjacent to the heated walls increases in thickness and natural convection starts to drive the hot liquid PCM upwards due to the density difference between the hotter and cooler liquid PCM. As melting progresses, the fluid circulation continues to grow increasing the melt fraction. Natural convection becomes dominant and the heat transfer coefficient from the heated surface to the PCM increases. This means that the power input is transferred from the wall to the PCM for a smaller temperature difference and the rate of increase of local wall surface temperature reduced.

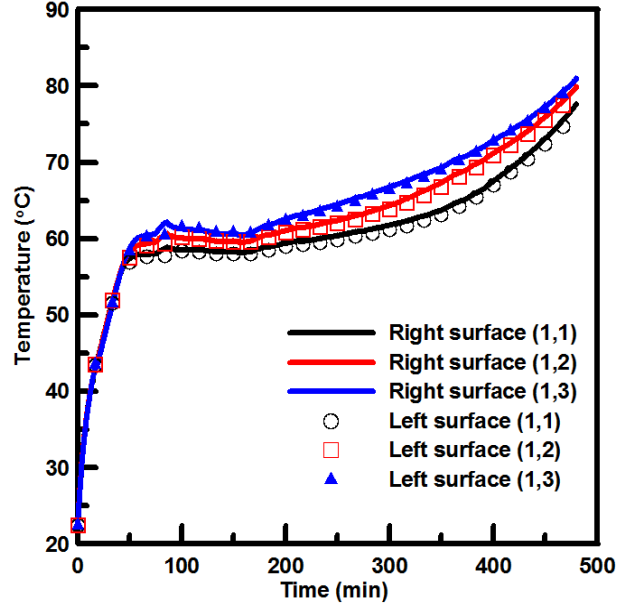


Figure 8. Measured heated wall surface temperatures in the vertical direction for heat flux,  $q''=960 \text{ W/m}^2$ .

The temperatures measured with the thermocouples inside the test cell are presented in Fig 9 for a heat flux  $q''=960 \text{ W/m}^2$ . During the early stages of the experiment, there is a uniform and moderate increase in the temperatures due to the PCM being solid and conduction being the only form of heat transfer. From Fig. 9, it can be seen that when the PCM adjacent to the heated walls is molten convection develops and the temperatures in the upper part of the test cell are generally higher than the temperatures in the lower part. The convection currents in the liquid PCM adjacent to the left and right heated walls result due to the increase in temperature due to the heat input. The heated less dense liquid rises up the wall and is deflected at the container top surface prior to flowing down the solid/liquid interface in the PCM. The left side flow is in the clockwise direction and the right-side flow is anticlockwise maintaining symmetry. At the solid/liquid interface heat is transferred from the warm liquid to the cooler solid PCM (causing it to melt) and cooling the liquid which becomes denser and sinks.

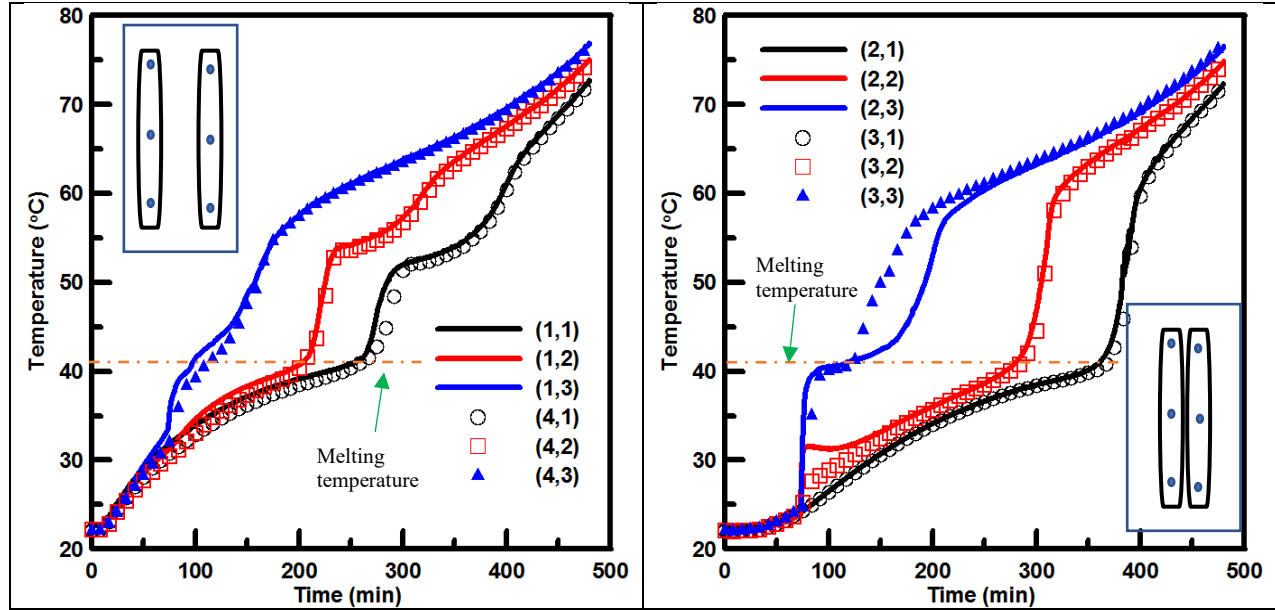


Figure 9. Measured temperatures at the 12 thermocouple locations within the test cell with time for a wall heat flux of  $q''=960 \text{ W/m}^2$ .

The natural convection in the liquid PCM contributes strongly to the melting process. As can be seen in Fig. 9 due to the natural convection in the liquid PCM the melting front progressed much faster at the top of the container than at the bottom. The slight differences between temperatures measured by thermocouples  $T_{(2,3)}$  and  $T_{(3,3)}$  result due to difficulty in mounting the top thermocouples at exactly the same location compared to the wall heaters. The pictures of the solid/liquid interface in the following section confirm the near symmetry of the melting process.


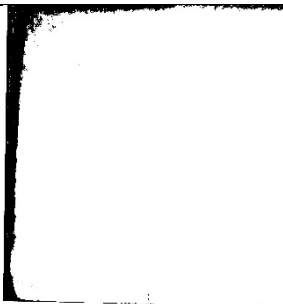

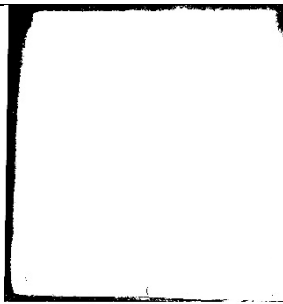



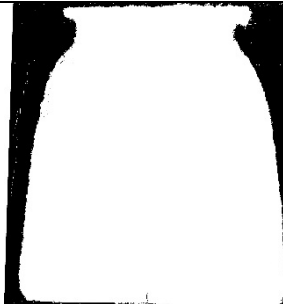

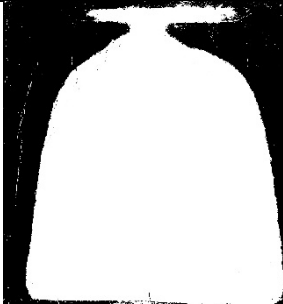
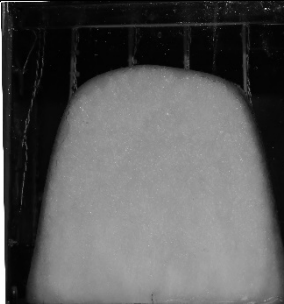
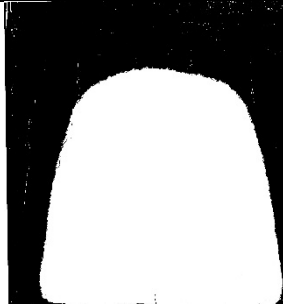
### Solid/liquid interface tracking

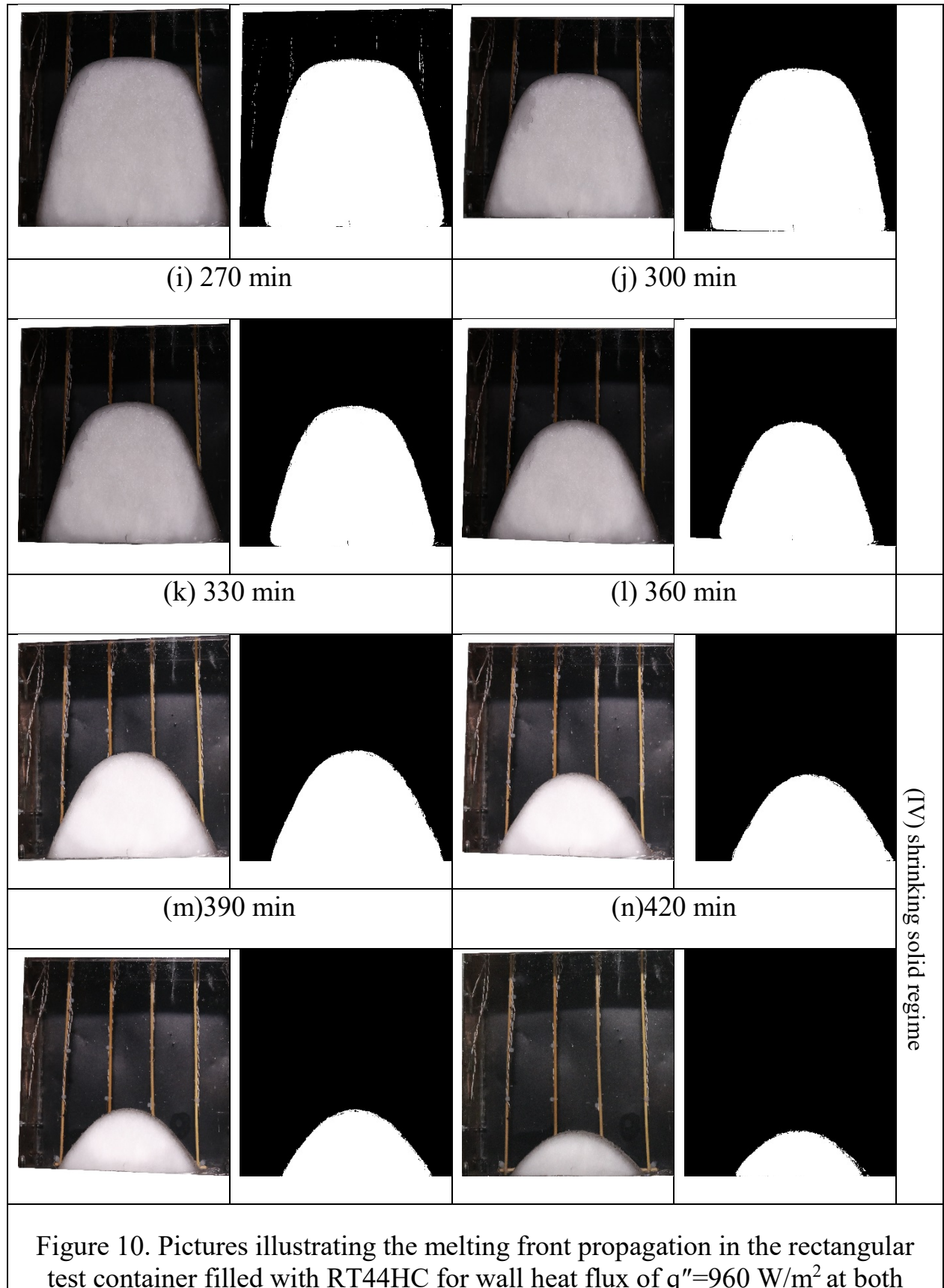
Fig.10 presents photographs taken every 30 minutes during the experiment (with a uniform wall heat flux of  $q''=960 \text{ W/m}^2$  imposed on the left and right walls) showing the progress of the solid/liquid interface during the melting of RT44HC. In these photographs, white and black areas represent the solid and liquid phases, respectively. The symmetrical nature of the melting process can be clearly seen. From Fig.10 the melting process can be characterizing into four distinct regimes (i)



conduction dominated melting [30-60 minutes], (ii) mixed convection-conduction melting [60-150 minutes], (iii) convection dominated melting prior to left and right-side flows meeting [150-300 minutes], (iv) convection dominated melting after left and right-side flows have met [300-480 minutes].

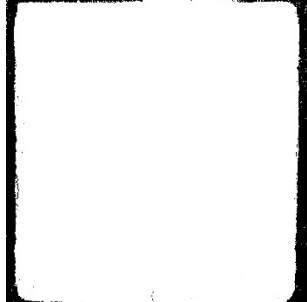
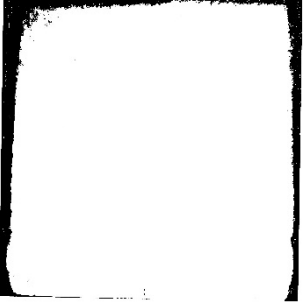
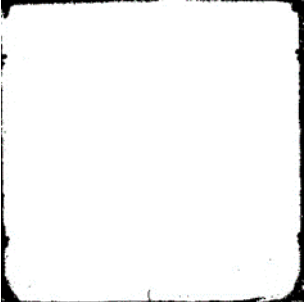
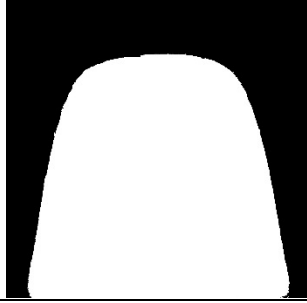
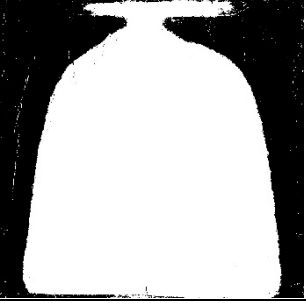
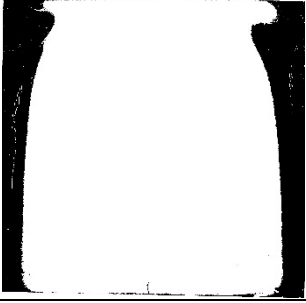
Up to 60 minutes the solid/liquid interface was almost vertical parallel to the heated plate due to heat transfer being predominantly by conduction. This mode of heat transfer prevailed while the viscous force was sufficient to suppress fluid motion (Fig.10 a and b). With the elapse of time, more RT44HC is heated and melts, the buoyancy force resulting from the increased temperature and reduction in density becomes sufficient to overcome the viscous force and natural convection occurs in the liquid region. The resulting convective flow leads to an increase in melting at the top of the container and an acceleration in the movement of the solid/liquid interface in this region compared to lower down on the heated wall. The flow changed direction at the top of the container impinging on the solid PCM and creating a concave curve at the top of the melt front seen in Fig.10 (c-e). As the melting progresses, natural convection intensifies and its effect on the melt front becomes more pronounced. The increasing curvature of the melt front in the upper part of the test cell provides conclusive evidence of this effect. The rapid change in the melt layer thickness at the top results from the flow changing direction and the hot fluid flowing along the underside of the top surface and impinging on the solid PCM at the top of the container. In the lower part of the test cell, the shape of the interface remains almost linear, its angle of tilt increases as the solid PCM shrinks. This pattern of melting continues until the solid PCM melts completely.

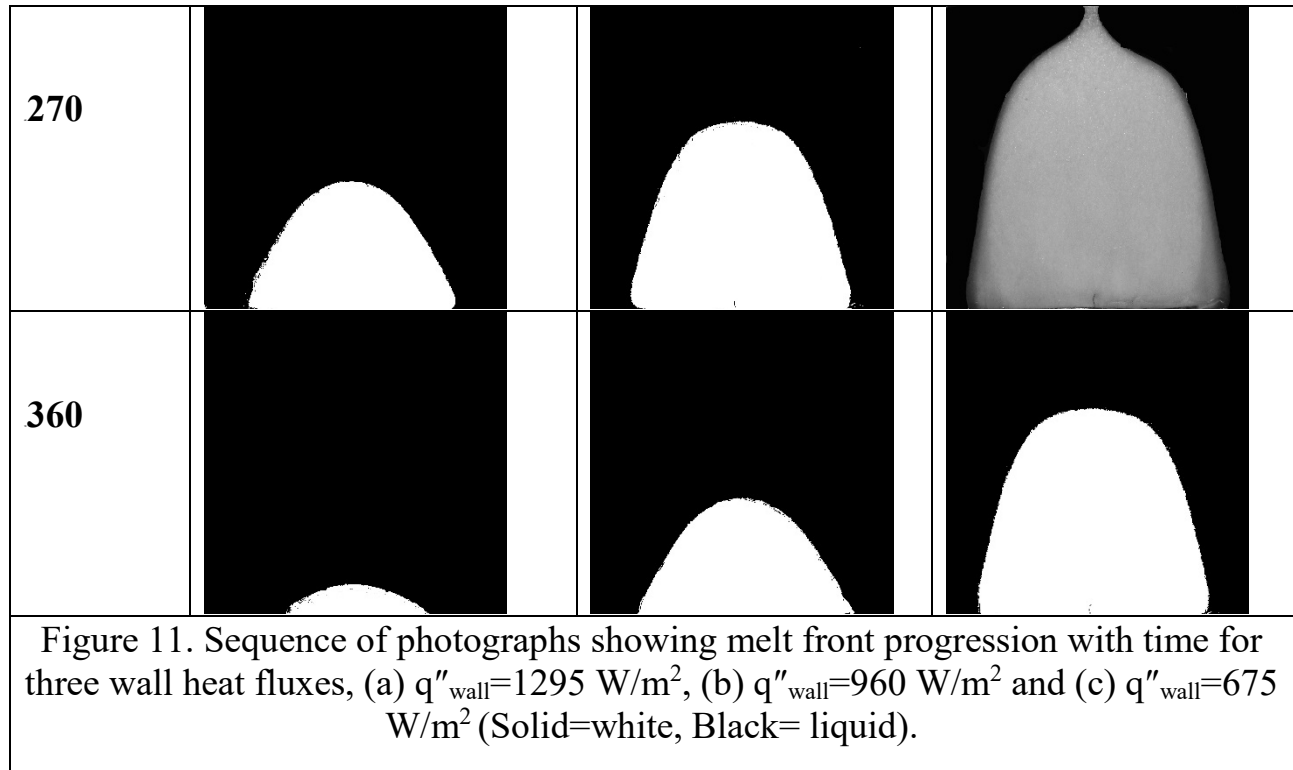
(a) 30 minutes		(b) 60 minutes		(I) Conduction Regime
				
(c) 90 minutes		(d) 120 minutes		(II) Transition regime
				
(e) 150 minutes		(f) 180 minutes		(III) Convection regime
				
(g) 210 minutes		(h) 240 minutes		



vertical walls. Black regions represent liquid PCM and white regions solid.

Fig.11 shows the melt front shapes at different times for three wall heat flux values  $q''_{\text{wall}}=1295 \text{ W/m}^2$ ,  $q''_{\text{wall}}=960 \text{ W/m}^2$  and  $q''_{\text{wall}}=675 \text{ W/m}^2$ . The volume of the liquid PCM regions at the top of the test cell grow due to the natural circulation of the liquid PCM until they unite in the middle and the remaining solid PCM is left in the middle at the base of the test cell. The remaining solid PCM continues to melt slowly, as the heated liquid PCM transports thermal energy to the middle of the test cell. As expected, melt front evolution is nearly symmetrical with similar profiles produced when different heat fluxes are imposed on both left and right walls. It can be seen that the melt front advances faster when the wall heat flux is increased.

Time (minutes)	(a) $q''_{\text{wall}}=1295 \text{ W/m}^2$	(b) $q''_{\text{wall}}=960 \text{ W/m}^2$	(c) $q''_{\text{wall}}=675 \text{ W/m}^2$
30			
150			



It can be seen in Fig.12 that, as the wall heat flux increases, the time for total melting decreases, due to the increased rate of heat transfer to the test cell. The increase in power input also led to an increase in the average temperature of both the PCM and the heating surface. Increasing the input power from  $675 \text{ W/m}^2$  to  $960 \text{ W/m}^2$  to  $1295 \text{ W/m}^2$  reduces the total time for the melting process by 27.27 % and 43.18 % respectively.

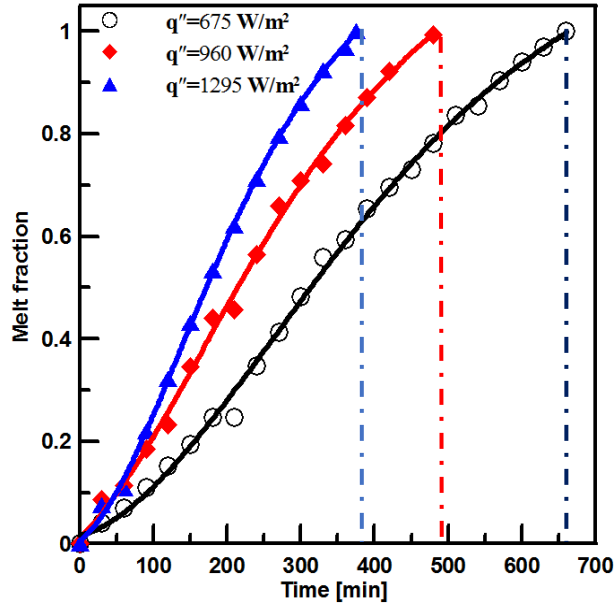


Figure 12. Melt fraction versus time for three different wall heat fluxes, 675, 960 and 1295 W/m<sup>2</sup>.

The hot wall temperature was evaluated by averaging thermocouples measurements along the vertical centre line of the copper wall. Fig.13 shows the temperature history along the hot wall for the three heat flux values used. It can be seen from Fig 13 that the hot wall temperature initially increases linearly following the experiment start-up. This shows that melting is determined by conduction in the initial stages of the experiments. This initial stage lasts for 40 min, 60 min and 90 min for the heat fluxes of 1295, 960 and 675 W/m<sup>2</sup>, respectively. The maximum wall temperatures measured in this stage are 63 °C, 60 °C and 55 °C for the three heat fluxes. The temperatures of the heated walls then remain constant due to the onset of natural convection in the liquid PCM. As time progresses, the temperatures of the heated walls start to increase rising slowly until the end of the melting process and the experiment.

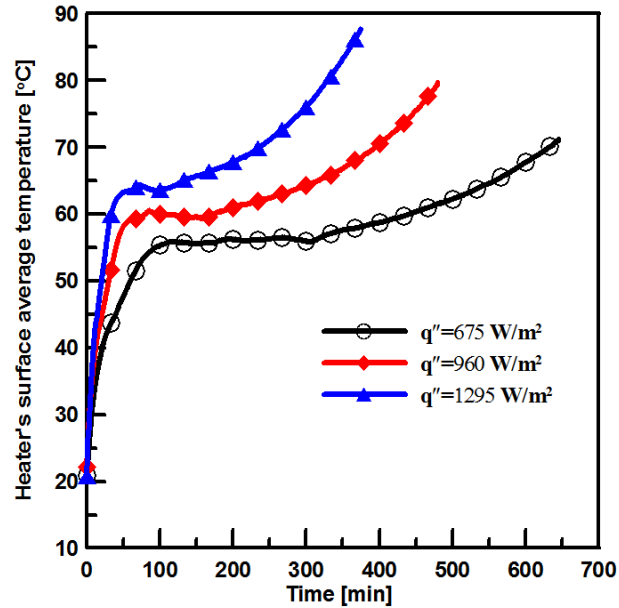


Figure13. The average temperature of the heated walls for the three different wall heat flux values  $q''_{\text{wall}}=675, 960$  and  $1295 \text{ W/m}^2$ .

From Fig.14 it can be seen that by the time all of the PCM melts the average PCM temperature is  $19^\circ\text{C}$  greater for a wall heat flux of  $960$  compared to  $675 \text{ W/m}^2$  and is  $33^\circ\text{C}$  greater for a wall heat flux of  $1295 \text{ W/m}^2$ .

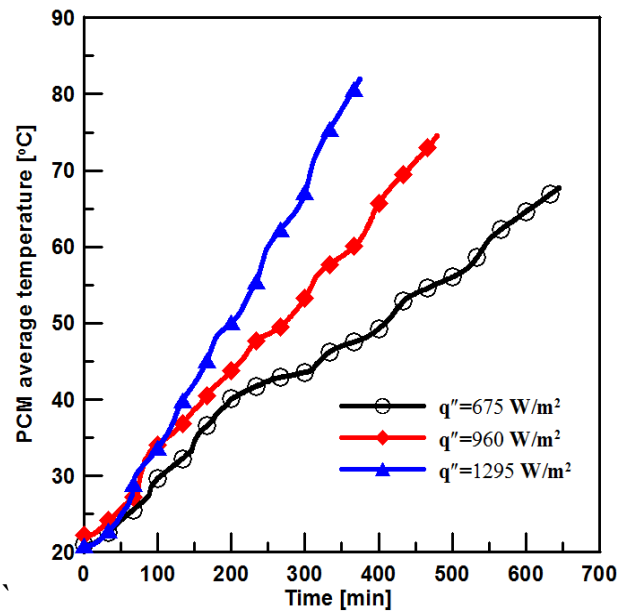


Figure 14. Average PCM temperature for the three different wall heat fluxes of  $675, 960$  and  $1295 \text{ W/m}^2$ .

## Front wall PCM test cell temperatures measured using an infrared camera

The temperatures measured using thermocouples reflect the temperatures at the thermocouple beads. To obtain the temperature distribution of the entire domain using thermocouples would be highly intrusive and influence system behaviour. An infrared camera was used to unobtrusively measure the temperature of the outer surface of the polycarbonate test cell.

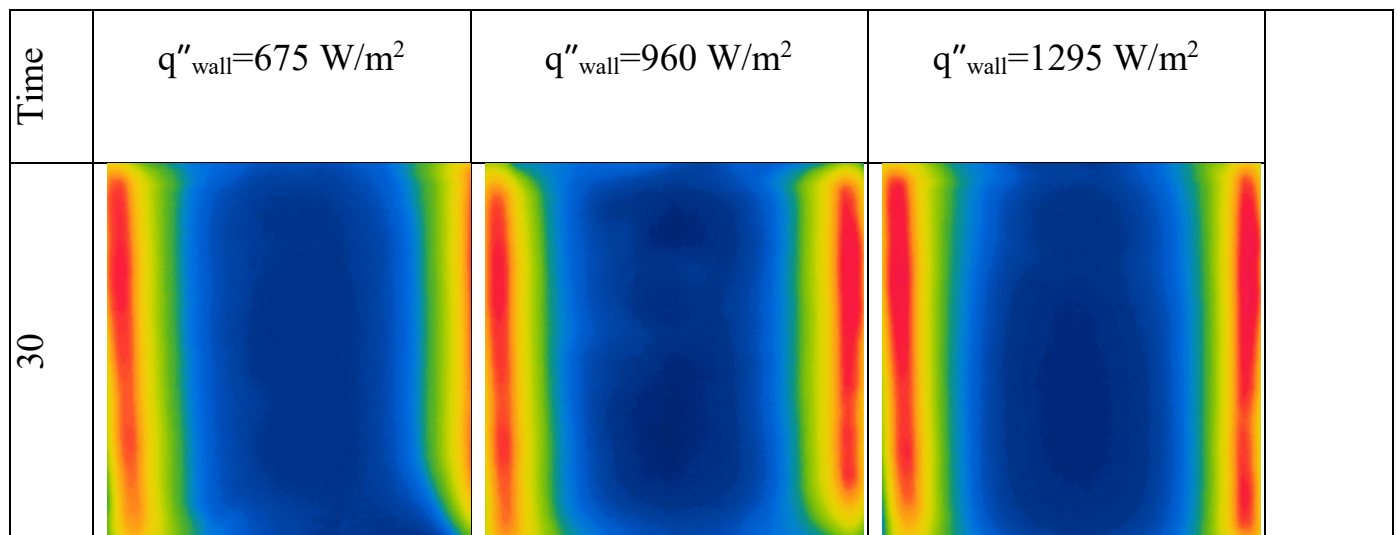
Fig.15 presents the IR images taken for the three different wall heat fluxes and illustrates how the temperature profile of the front surface of the PCM test cell changed during the experiment. Melting starts parallel to the hot walls (Right and left-hand sides) and progress from the top right and left-hand corners towards the centre of the test cell. Temperature differences are sufficient to produce clockwise and anticlockwise convection currents. As time elapses temperatures increases and the density of the liquid PCM adjacent to the hot walls decreases and the liquid PCM adjacent to the hot wall rises until it reaches the top of the melt layer.

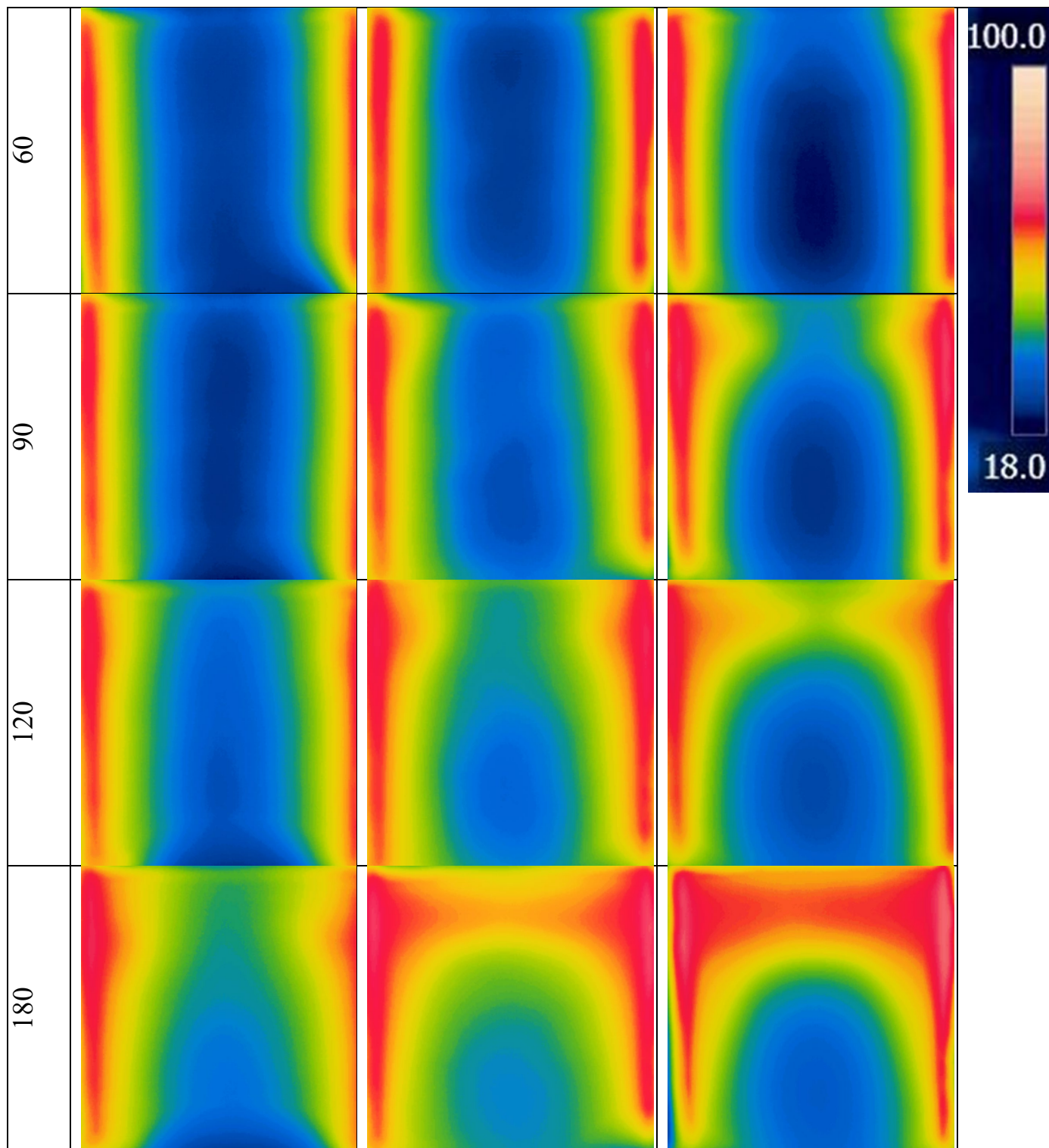
It then flows horizontally before descending along the solid/liquid interface reducing in temperature. The change in direction from vertical to horizontal flow at the top of the test cell leads to the inclination of the temperature contours. It can also be seen that as the wall heat flux increases the higher temperature of the descending liquid at the top surface of the melt layer increases the local heat transfer rate at the solid/liquid interface, melting the top part of the solid PCM more rapidly.

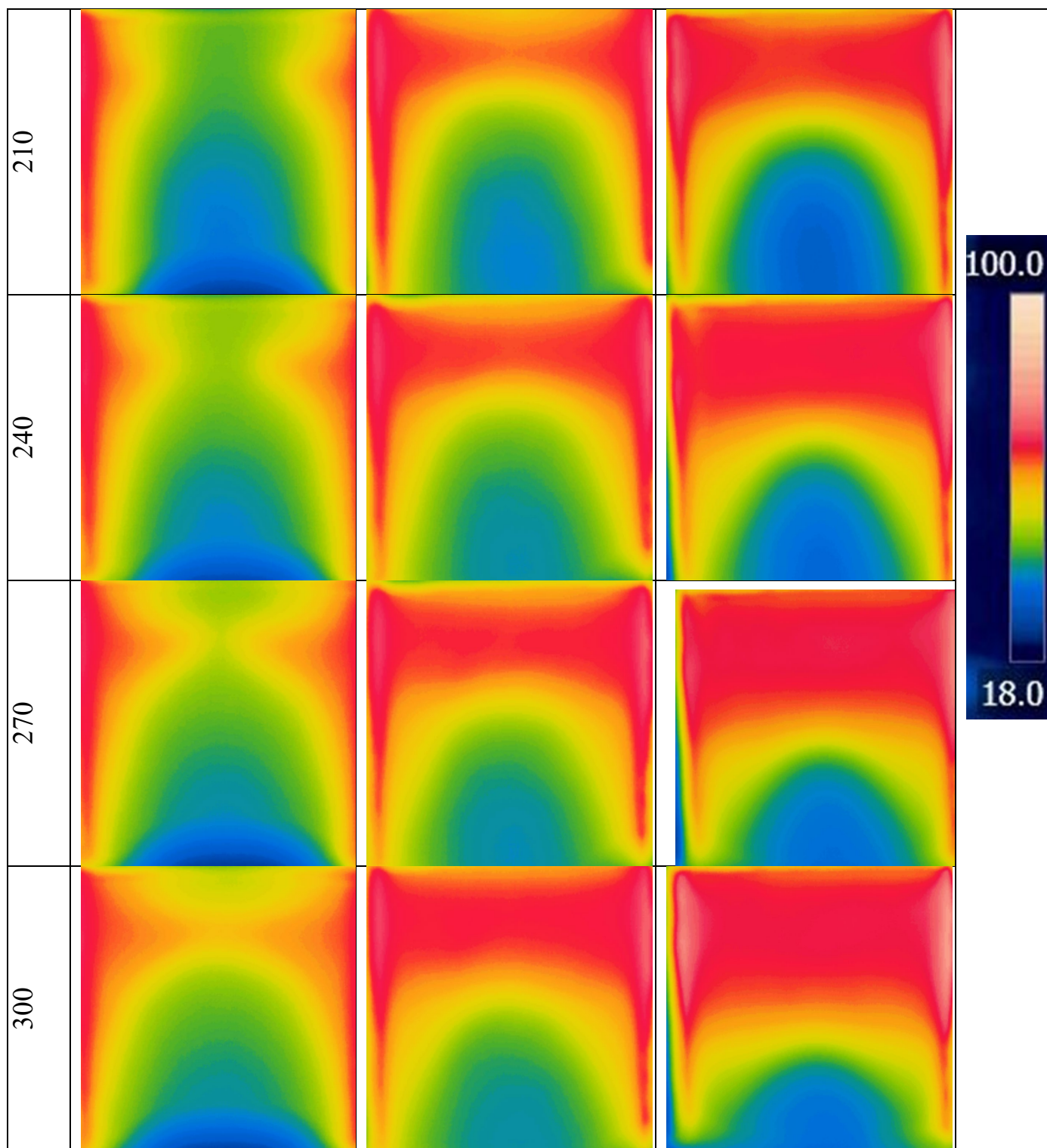
When sufficient PCM melts the IR pictures show a nearly uniform temperature region in the upper part of the liquid PCM and a region with a temperature gradient in the lower part of the liquid PCM. This indicates two distinct regions with different strengths of convection currents in the upper and lower parts of the test



cell. Although there is not a sharp boundary between these two regions, they can be defined by a virtual horizontal surface drawn level with the top point of the solid PCM. A strong circulation exists in the liquid PCM below the virtual horizontal surface with a weak circulation in the nearly uniform temperature liquid PCM above it. The majority of the ascending hot flow adjacent to the heated walls is drawn to the left and right by the descending flow resulting from the increase in density due to heat transfer to the colder solid PCM. Change in fluid density at the hot and cold surfaces generate the strong convective circulation below the virtual horizontal surface level with the top of the solid PCM. The remainder of the ascending flow at the heated walls continues to rise until it impinges on the top surface. Since there is no cool solid PCM above the virtual horizontal surface, the fluid circulation is not strengthened above the virtual horizontal line. The upper uniform temperature region at the top of the test cell is confirmation of the very weak circulation in this area of the liquid PCM. As the solid PCM melts and shrinks, the virtual horizontal surface descends, and the region of limited fluid flow grows. This virtual surface eventually becomes coincident with the floor of the test cell when the solid PCM melts completely [31].









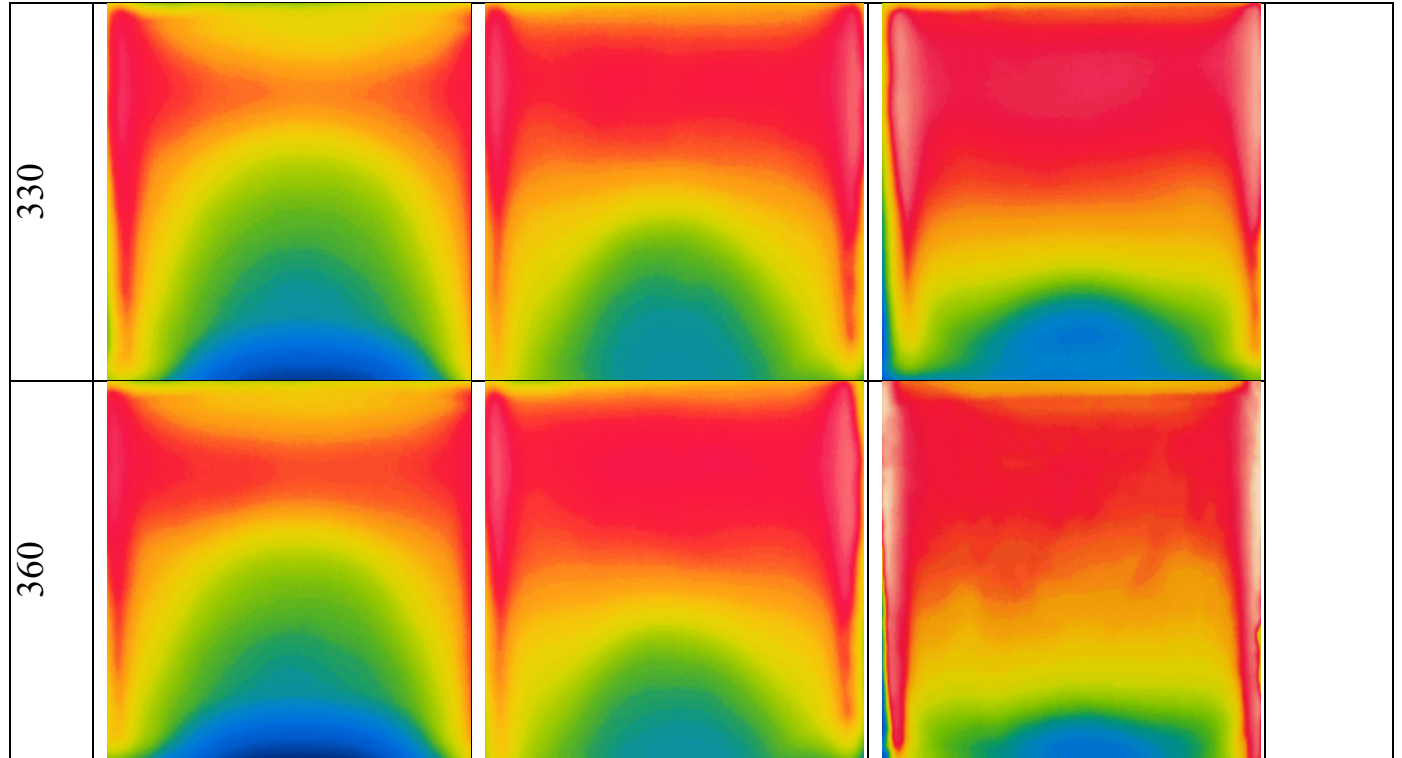


Figure 15. Infrared images of the front surface of a rectangular cross-section test cell filled with PCM RT44HC during melting with three different applied wall heat fluxes.

Fig.16 presents the differences in temperature recorded by thermocouples located in positions  $T_{(i,3)}$  (top of the vertical mid-plane of the test cell) and  $T_{(i,1)}$  (bottom of the vertical mid-plane of the test cell) and  $T_{(i,2)}$  (middle of vertical mid-plane of the test cell) for the three values of wall heat flux.

In the first 50 minutes, the rise in the measured temperature differences are similar for all flux values due to conduction in the solid PCM being the main heat transfer mechanism. At  $t=50$  minutes, the thermocouples in the upper location show a much greater temperature rise than those in the middle and bottom locations due to the onset of natural convection in the melted liquid PCM, which increases the local heat transfer rate between the solid and liquid PCM in the upper section of the test cell. The value of the increase in temperature difference is an indicator of the strength of the local heat transfer rate at the solid-liquid interface.

The higher values of wall heat flux increase the rate at which the temperature difference is established suggesting a faster onset of convection and a higher rate of convection at higher wall heat fluxes. When the RT44HC is melted fully, natural convection increases mixing in the liquid paraffin, leading to the gradual decrease in the temperature difference.

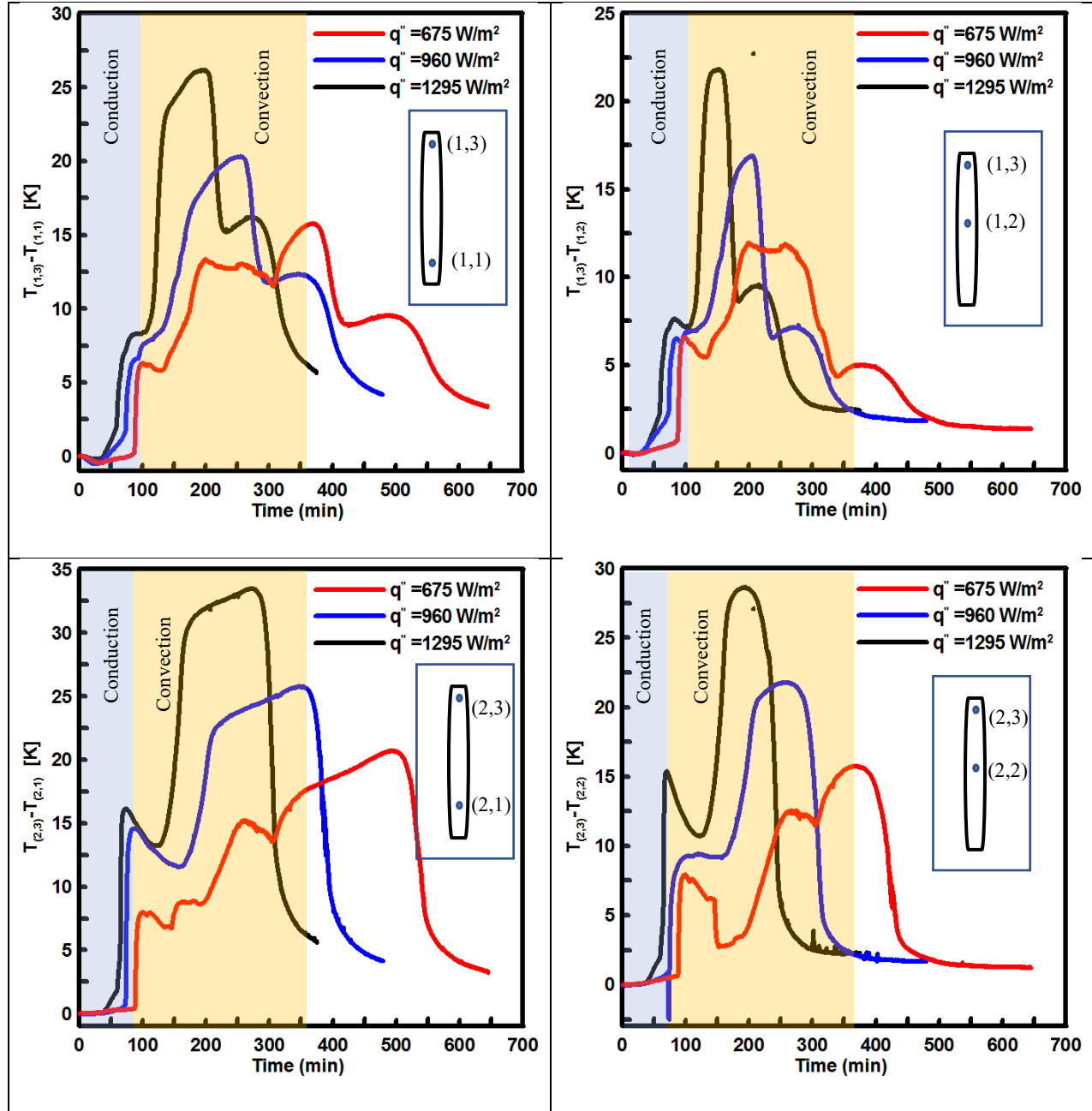
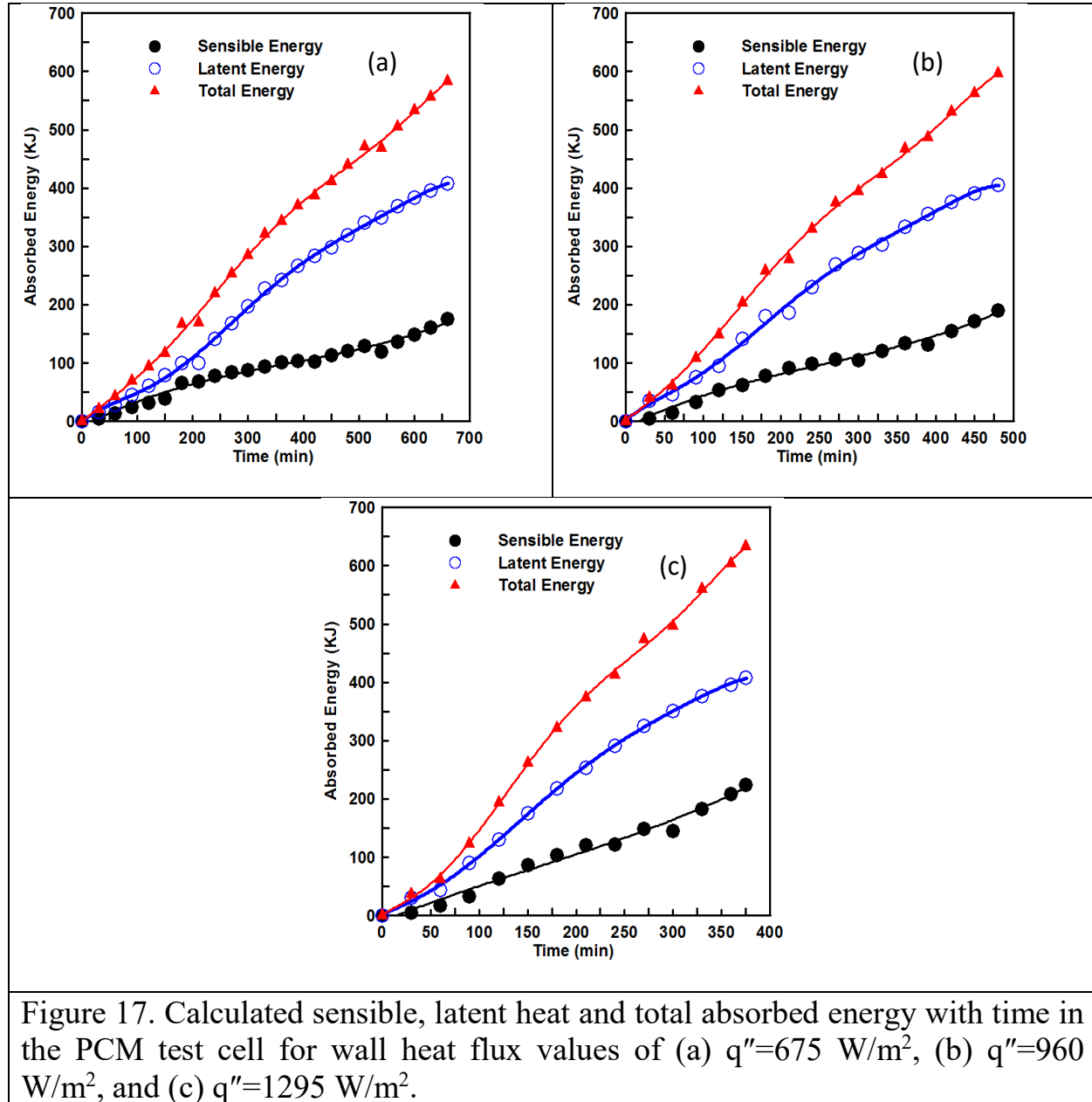


Figure 16. Variation of the measured temperature difference recorded by thermocouples located at position  $T_{(i,3)}$  (top) and  $T_{(i,1)}$  (bottom) and  $T_{(i,2)}$  (middle) for three values of wall heat flux.

Fig.17 shows the calculated increase in sensible, latent and total stored energy within the test cell unit at every 30 min for different wall heat flux values. As can be seen in Fig.17, the contribution of latent heat to the total heat absorbed is much greater than sensible heat. As expected for all values of wall heat flux, the

maximum values of absorbed latent heat are equal since they are a function of the storage unit volume which is constant for all experiments. It can be observed that the values of the maximum total energy absorbed change slightly due to the change of hot wall temperature which is the result of different values of heat flux.



In order to characterize the overall heat transfer during melting, the variation of surface-averaged Nusselt numbers was calculated at various times for the three

wall heat flux values is presented in Fig.18. The variation of the Nusselt number indicates the strength of the convective heat transfer changes during the melting process. In each experiment, the Nusselt number is small initially indicating heat transfer is conduction dominated when melting initiates, the value of the Nusselt number increase gradually, later, the length of the solid-liquid boundary reduces and the Nusselt number reduces for the remainder of the melting process. This reduction in Nusselt number indicates the weakening of the convective current which results due to the increase in bulk temperature of the liquid PCM, reduction in temperature gradient and the reduction in the length of the melting front[32].

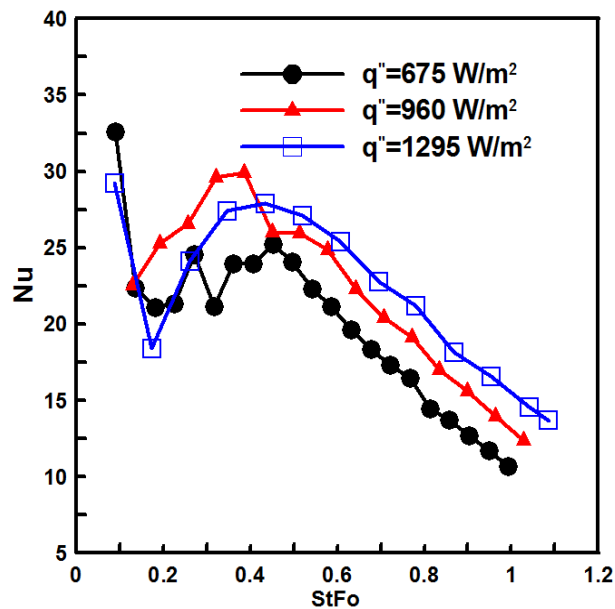


Figure 18. Variation of the Nusselt number with wall heat flux.

## Conclusions

The melting of phase change material (PCM) RT44HC has been explored experimentally in a vertically oriented rectangular cross-section test cell to understand the effect of different values of wall heat flux on the development of the melt fraction, PCM average temperature, amount of absorbed energy, temperature distributions, heated wall surface temperature and the Nusselt number.



Images of the melting process and the instantaneous temperature distribution at the vertical mid-plane of the test cell were recorded. The images of the melting process were analysed using an image processing technique to measure the melt fraction development with time. The development of the melt front and recorded temperature distributions were employed to analyse the dominant mode of heat transfer during the different stages of melting. It was observed, at higher values of wall heat flux, the average temperature of the heater's surface and the PCM increased and the total melting time reduced, this was expected due to the greater rate of heat input. Increasing the input power from  $675 \text{ W/m}^2$  to  $960 \text{ W/m}^2$  to  $1295 \text{ W/m}^2$  reduces the total time for the melting process by 27.27 % and 43.18 % respectively. Conduction is the dominant mode of heat transfer during the early stage of melting which is followed by a short transition period before convection dominates the remainder of the melting process. The experimental measurements provide a set of benchmark data suitable for validation of numerical simulation tools.

## **Acknowledgements**

The authors are grateful to the Engineering and Physical Sciences Research Council (EPSRC) for funding this work through Grant references EP/N021304/1 and EP/K011847/1.

## **Analysis of Experimental Uncertainty**

### **Experimental uncertainty analysis**

To estimate the uncertainty in the results. The uncertainties in the primary measurements are required. The experimental uncertainty analysis was then performed based on the methods described in [33]. Assuming that the final results

are derived from independent variables  $y_1, y_2, \dots, y_n$ . The uncertainty of result  $W$  is obtained by appropriately combining the uncertainty of the independent variables  $W(y_i)$  as follow:

$$K = f(y_1, y_2, \dots, y_n) \quad (12)$$

$$W(K) = \sqrt{\sum_{i=1}^n \left( \frac{\partial f}{\partial y_i} W(y_i) \right)^2} \quad (13)$$

The expected uncertainties in the calculated results, as well as the uncertainties in the independent variables, are given in Table 3.

<b>Table 3 Uncertainties of measured and calculated variable</b>	
<b>Variables (Units)</b>	<b>Uncertainty</b>
Height or positions (mm)	$\pm 0.5$
Mass (g)	$\pm 1.0$
Wall or PCM temperature ( $^{\circ}\text{C}$ )	$\pm 0.3$
Voltage (volts)	0.05%
Resistance (ohm)	$\pm 0.1$
Heater's power (W)	0.2
Liquid volume fraction	3.8 %
Heat transfer coefficient ( $\text{W/m}^2 \text{K}$ )	7.3 %
Nusselt number	7.8 %

## References

- [1] International Energy Agency, Medium-Term Renewable Energy Market Report 2016, (2016) 278. doi:10.1787/9789264188471-en.
- [2] Z. Zhao, M.T. Arif, A.M. T O, Solar thermal energy with molten-salt storage for residential heating application, Energy Procedia. 110 (2017) 243–249. doi:10.1016/j.egypro.2017.03.134.
- [3] B. Xu, P. Li, C. Chan, Application of phase change materials for thermal energy storage in concentrated solar thermal power plants: A review to recent developments, Appl. Energy. 160 (2015) 286–307. doi:10.1016/J.APENERGY.2015.09.016.
- [4] N.S. Dhaidan, J.M. Khodadadi, Melting and convection of phase change

- materials in different shape containers: A review, *Renew. Sustain. Energy Rev.* 43 (2015) 449–477. doi:10.1016/j.rser.2014.11.017.
- [5] S. Jegadheeswaran, S.D. Pohekar, Performance enhancement in latent heat thermal storage system: A review, *Renew. Sustain. Energy Rev.* 13 (2009) 2225–2244. doi:10.1016/J.RSER.2009.06.024.
  - [6] F. Agyenim, N. Hewitt, P. Eames, M. Smyth, A review of materials, heat transfer and phase change problem formulation for latent heat thermal energy storage systems (LHTESS), *Renew. Sustain. Energy Rev.* 14 (2010) 615–628. doi:10.1016/j.rser.2009.10.015.
  - [7] M. Fadl, P. Eames, A comparative study of the effect of wall heat flux on melting and heat transfer characteristics in phase change material thermal energy stores arranged vertically and horizontally: 9<sup>th</sup> Ed. Int. SOLARIS Conf., IOP Conference Series: Materials Science and Engineering (MSE), Chengdu, China, 2018. doi:10.1088/issn.1757-899X.
  - [8] M. Fadl, P. Eames, A Numerical Investigation into the Heat Transfer and Melting Process of Lauric Acid in a Rectangular Enclosure with Three Values of Wall Heat Flux, *Energy Procedia.* 158 (2019) 4502–4509. doi:10.1016/J.EGYPRO.2019.01.761.
  - [9] A. Dinker, M. Agarwal, G.D. Agarwal, Heat storage materials, geometry and applications: A review, *J. Energy Inst.* 90 (2017) 1–11. doi:10.1016/J.JOEI.2015.10.002.
  - [10] B. Šarler, Stefan's work on solid-liquid phase changes, *Eng. Anal. Bound. Elem.* 16 (1995) 83–92. doi:10.1016/0955-7997(95)00047-X.
  - [11] A. Yadav, S. Samir, Experimental and numerical investigation of spatiotemporal characteristics of thermal energy storage system in a rectangular enclosure, *J. Energy Storage.* 21 (2019) 405–417. doi:10.1016/j.est.2018.12.005.
  - [12] D. Pal, Y.K. Joshi, Melting in a side heated tall enclosure by a uniformly dissipating heat source, *Int. J. Heat Mass Transf.* 44 (2001) 375–387. doi:10.1016/S0017-9310(00)00116-2.
  - [13] M. Bashar, K. Siddiqui, Experimental investigation of transient melting and heat transfer behavior of nanoparticle-enriched PCM in a rectangular enclosure, *J. Energy Storage.* 18 (2018) 485–497. doi:10.1016/J.EST.2018.06.006.
  - [14] B. Kamkari, H. Shokouhmand, Experimental investigation of phase change material melting in rectangular enclosures with horizontal partial fins, *Int. J. Heat Mass Transf.* 78 (2014) 839–851.

- doi:10.1016/j.ijheatmasstransfer.2014.07.056.
- [15] N.S. Dhaidan, J.M. Khodadadi, T.A. Al-Hattab, S.M. Al-Mashat, Experimental and numerical investigation of melting of phase change material/nanoparticle suspensions in a square container subjected to a constant heat flux, *Int. J. Heat Mass Transf.* 66 (2013) 672–683. doi:10.1016/j.ijheatmasstransfer.2013.06.057.
  - [16] B. Kamkari, H. Shokouhmand, F. Bruno, Experimental investigation of the effect of inclination angle on convection-driven melting of phase change material in a rectangular enclosure, *Int. J. Heat Mass Transf.* 72 (2014) 186–200. doi:10.1016/j.ijheatmasstransfer.2014.01.014.
  - [17] D. Yanxia, Y. Yanping, J. Daiyong, C. Baoyi, M. Jinfeng, Experimental investigation on melting characteristics of ethanolamine-water binary mixture used as PCM, *Int. Commun. Heat Mass Transf.* 34 (2007) 1056–1063. doi:10.1016/j.icheatmasstransfer.2007.07.002.
  - [18] F.A. Hamad, E. Egelle, K. Cummings, P. Russell, Investigation of the melting process of polyethylene glycol 1500 (PEG 1500) in a rectangular enclosure, *Int. J. Heat Mass Transf.* 114 (2017) 1234–1247. doi:10.1016/j.ijheatmasstransfer.2017.07.014.
  - [19] S. Motahar, A.A. Alemrajabi, R. Khodabandeh, Experimental investigation on heat transfer characteristics during melting of a phase change material with dispersed TiO<sub>2</sub> nanoparticles in a rectangular enclosure, *Int. J. Heat Mass Transf.* 109 (2017) 134–146. doi:10.1016/j.ijheatmasstransfer.2017.01.109.
  - [20] B.J. Jones, D. Sun, S. Krishnan, S. V. Garimella, Experimental and numerical study of melting in a cylinder, *Int. J. Heat Mass Transf.* 49 (2006) 2724–2738. doi:10.1016/J.IJHEATMASSTRANSFER.2006.01.006.
  - [21] Plastic Acrylic Sheets. <https://www.sheetplastics.co.uk/> (accessed February 21, 2018).
  - [22] Copper Sheet. <https://www.themetalstore.co.uk> (accessed February 21, 2018).
  - [23] Kingspan Insulation UK, Kingspan Kooltherm,. <https://www.insulationsuperstore.co.uk> (accessed February 2, 2018).
  - [24] dataTaker- DT85 Data Logger. <http://www.datataker.com/DT85.php> (accessed February 2, 2018).
  - [25] Canon, Canon EOS 1100D. <https://www.canon.co.uk>. (accessed February 21, 2018).

- [26] FLIR B-Series Thermal Camera. <http://www.flir.co.uk> (accessed February 21, 2018).
- [27] H. Shokouhmand, B. Kamkari, Experimental investigation on melting heat transfer characteristics of lauric acid in a rectangular thermal storage unit, *Exp. Therm. Fluid Sci.* 50 (2013) 201–222. doi:10.1016/j.expthermflusci.2013.06.010.
- [28] Rubitherm GmbH, (2014). <https://www.rubitherm.eu/> (accessed February 21, 2018).
- [29] TA Instruments, Differential Scanning Calorimeters, (2015). <http://www.tainstruments.com> (accessed February 21, 2018).
- [30] Image Processing, Mathworks. (2016). <https://uk.mathworks.com/> (accessed February 21, 2018).
- [31] H. Shokouhmand, B. Kamkari, Experimental investigation on melting heat transfer characteristics of lauric acid in a rectangular thermal storage unit, *Exp. Therm. Fluid Sci.* 50 (2013) 201–222. doi:10.1016/j.expthermflusci.2013.06.010.
- [32] M.H. Joneidi, M.J. Hosseini, A.A. Ranjbar, R. Bahrampoury, Experimental investigation of phase change in a cavity for varying heat flux and inclination angles, *Exp. Therm. Fluid Sci.* 88 (2017) 594–607. doi:10.1016/j.expthermflusci.2017.07.017.
- [33] R.J. Moffat, Describing the uncertainties in experimental results, *Exp. Therm. Fluid Sci.* 1 (1988) 3–17. doi:10.1016/0894-1777(88)90043-X.

## Nomenclature

$A_w$	the cross-sectional area of the hot wall [ $m^2$ ]
$C$	specific heat at constant pressure [ $kJ/kg\ K$ ]
$f$	liquid fraction percentage
$H$	Hight of the test cell [ $m$ ]
$h_{latent}$	latent heat [ $kJ/kg$ ]
$h$	heat transfer coefficient [ $W/m^2\ K$ ]
$I$	electric current [ $amp$ ]
$k$	thermal conductivity [ $W/m\ K$ ]
$L$	length of the heating plate [ $m$ ]
$M$	mass [ $kg$ ]
$n$	number of thermocouples
$NP_0$	number of pixels with 0 value

$NP_t$	total number of pixels
Nu	Nusselt number
$Q_{\text{sensible}}$	sensible absorbed energy [kJ]
$Q_{\text{latent}}$	total absorbed energy [kJ]
$q''$	heat flux [ $\text{W}/\text{m}^2$ ]
t	time (t)
T	temperature ( $^{\circ}\text{C}$ )
$T_{\text{m1}}$	the onset of melting temperature ( $^{\circ}\text{C}$ )
$T_{\text{m2}}$	the endset of melting temperature ( $^{\circ}\text{C}$ )
$T_{\text{mean}}$	mean temperature ( $^{\circ}\text{C}$ )
v	volume [ $\text{m}^3$ ]
V	electric potential [volt]
W	the width of the heating plate [m]
<i>Greek Symbols</i>	
$\beta$	expansion coefficient [ $1/\text{K}$ ]
$\mu$	dynamic viscosity [ $\text{kg}/\text{m s}$ ]
$\rho$	density, [ $\text{kg}/\text{m}^3$ ]
Subscripts	
i	initial
s	solid
w	wall
Abbreviations	
PCMs	phase change materials
liq	liquid
DSLR	digital single-lens reflex